UNIVERSITY OF CALIFORNIA
RIVERSIDE

A Seismic Refraction Investigation of the Salton Sea Geothermal Area, Imperial Valley, California

A Thesis submitted in partial satisfaction
of the requirements for the degree of

Master of Science

in

Geological Sciences

by

Robert Bruce Frith

December, 1978

Thesis Committee:

Dr. Shawn Biehler, Chairman

Dr. Lewis H. Cohen

Dr. Donald J. Stierman

DISCLAIMER

The thesis of Robert Bruce Frith is approved:

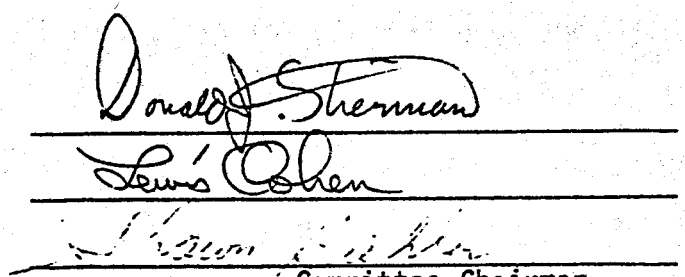

Committee Chairman

University of California, Riverside
December, 1978

ABSTRACT OF THE THESIS

A Seismic Refraction Investigation of the Salton Sea Geothermal Area, Imperial Valley, California

by

Robert Bruce Frith

Master of Science Graduate Program in Geological Sciences

University of California, Riverside, December 1978

Professor Shawn Biehler, Chairman

Seven seismic refraction profiles and four long-distance refraction shots have been used to investigate the Salton Sea geothermal area. From these data, two models of the geothermal and adjacent area are proposed. Model 1 proposes a basement high within the geothermal area trending parallel to the axis of the Imperial Valley. Model 2 assumes a horizontal basement in the E-W direction, and proposes a seismic velocity gradient that increases the apparent basement velocity from east to west approximately 15% within the geothermal area. Both models propose basement dip of 3 degrees to the south, yielding a thickness of sediments of 6.6 km near Brawley, California, in the center of the Imperial Valley. Based on offsets inferred in the sedimentary seismic layers of the geothermal area, two NW-SE trending fault zones are proposed. The respective locations are 3 km east and

2 km south of Obsidian Butte, the southernmost of five volcanic domes at the southeastern tip of the Salton Sea. A third fault zone, also trending NW-SW, might exist at Obsidian Butte.

Sedimentary seismic velocities reported from throughout the Imperial Valley are similar to the sedimentary seismic velocities found in the geothermal area. In particular, sedimentary seismic velocities reported from the center of the valley agree very closely with sedimentary seismic velocities of the geothermal area. Basement velocities reported along the center and margins of the valley average 6.2 and 5.3 km/sec respectively. The occurrence of high basement velocities along the center of the valley relative to the valley margins is interpreted as the expression of a more basic rock type at the valley center.

Emergent high amplitude secondary arrivals observed beginning near 8.2 sec on a N-S long-distance record are consistent with reflections from basement, and arrivals beginning at 8.6 sec are consistent with reflections from a horizon on the order of 21 km deep. The arrivals beginning near 8.6 sec are interpreted as reflections from the Mohorovicic discontinuity.

ACKNOWLEDGEMENTS

I would like to express my thanks to the student members and staff of IGPP for their assistance in data collection and final presentation. I am indebted to the members of my thesis committee for their constructive criticisms and review of this work. I am especially grateful to Shawn Biehler for his guidance, support, patience and understanding throughout this project.

Financial assistance was provided by LLL Intramural Order #8338305 and NSF grant #AER 72-03551.

TABLE OF CONTENTS

LIST OF TABLES

LIST OF FIGURES

INTRODUCTION AND GEOLOGIC SETTING

Within the Imperial Valley of southern California, the Salton Sea geothermal area is one of several expressions of a large geophysical anomaly related to crustal spreading. This area, possessing large reservoirs of hot liquids, is a candidate for extraction of geothermal energy. The object of this study was to use seismic refraction to investigate the known geothermal zone and adjacent areas in preparation for such energy resource development.

The Salton Sea geothermal area is located at the southeastern tip of the Salton Sea, in the Imperial Valley of southern California (Figure 1). The Imperial Valley, itself a portion of the Salton Trough, is a broad structural depression containing lacustrine and deltaic silts, sand and gravels of late Tertiary age, and thick Quaternary alluvium and lake sediments (Dibblee, 1954). The margins of the valley are step-faulted, with Mesozoic or older granitic and metasedimentary basement rocks comprising the bordering mountains (Elders et al., 1972) (Figure 1).

Associated with the geothermal area are positive gravity and magnetic anomalies, high heat flow, and recent volcanism (Elders et al., 1972). The geothermal area also experiences earthquake swarms (Gilpin, 1977; Hill, 1975). These characteristics are consistent with the suggestion that the Imperial Valley is the northern continuation of the Gulf of California tectonic province (Elders et al., 1972).

A crustal spreading center within the geothermal area has been postulated by Elders et al. (1972). The proposed spreading center

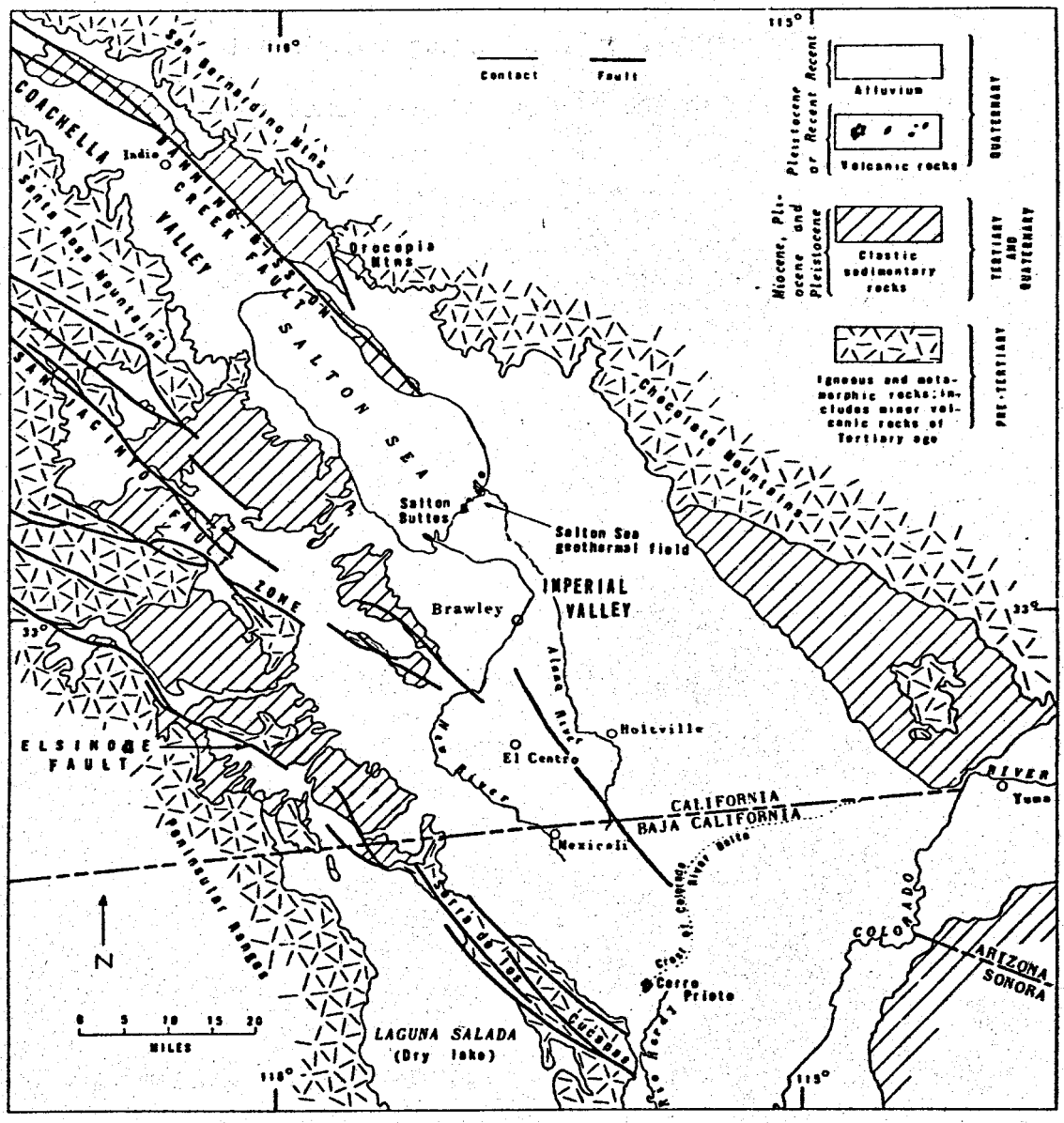

Figure 1

Geologic Map of the Salton Trough
(after Robinson et al., 1976)

is located near five rhyolite domes (known as the Salton Buttes) (Figure 1). These domes were extruded through the sediments between 16,000 and 50,000 years ago (Muffler and White, 1969). Abundant xenoliths, most commonly basalt and granite, provide a "grab sample" of the rocks beneath the valley (Elders, et al., 1972). The domes are spaced approximately 2 km apart along a northeast trend (Robinson, et al., 1976). The southern most of these domes is known locally as Obsidian Butte.

PREVIOUS INVESTIGATIONS

The earliest geophysical study of the geothermal area was a vertical intensity ground magnetic survey of the Salton Buttes conducted by Kelley and Soske (1936). They concluded that the steep magnetic gradients observed near these domes were the expression of a sloping underground igneous mass. No quantitative discussion was given. Based on the results of an aeromagnetic survey of the same area, Griscom and Muffler (1971) propose an underground magnetic mass as the cause of a linear magnetic high trending NW-SE through the geothermal area. They calculated a depth to the mass of 2.1 km near Obsidian Butte.

A gravity map of the Salton Trough was prepared by Biehler (1964). A positive gravity anomaly was observed coincident with the Salton volcanic domes. Applying the half-width method to the anomaly, Biehler concluded that a spherical body 3 to 5 km in radius at a depth of approximately 6 km could explain the observed gravity anomaly.

The presence of several faults has been reported in geophysical studies of the geothermal and adjacent areas. Based on an examination of well-core data and cuttings from test wells within the geothermal area, Randall (1974) postulated several faults. Based on the results of resistivity measurements in the geothermal area, Meidav (1968) and Meidav et al. (1974) proposed the existence of six faults. Active faulting and occurrences of earthquake swarms have also been reported within the geothermal area (Gilpin, 1977; Johnson and Hadley, 1976; Hill, 1975; and Savage et al., 1974).

Three seismic refraction studies have been conducted previously in the Imperial Valley (Biehler, 1964; Biehler et al., 1964; and Kovach et al., 1962). The locations of the seismic profiles are shown in Figure 2 (indicated by numbers 1-8) and a summary of seismic velocity models based on these profiles is given in Table 1. The seismic models near the eastern flank of the valley (East Highline Canal-3, Coachella Canal-2, Glamis-Ogilby-4), the Mexican Border-5,6, and the western flank of the valley (Plaster City-7, Superstition Hills-4,8) are provided by Kovach et al. (1962). The East Highline Canal profile proposes basement depth of 3.05 km and a velocity of 5.5 km/sec near the east flank of the valley. Additional seismic velocity models near the eastern flank of the valley (Frink), the center (Westmoreland), and western flank of the valley (Truckhaven) are provided by Biehler (1964) and Biehler et al. (1964). The Frink profile proposes basement depth of 2.23 km and velocity of 5.38 km/sec near the eastern flank of the valley. The Truckhaven profile proposes a depth of 1.69 km and velocity of 5.39 km/sec near the western flank of the valley. The Westmoreland profile porposes a basement velocity of 6.4 km/sec, and extrapolating basement toward the center of the valley yielded a depth of approximately 6 km.

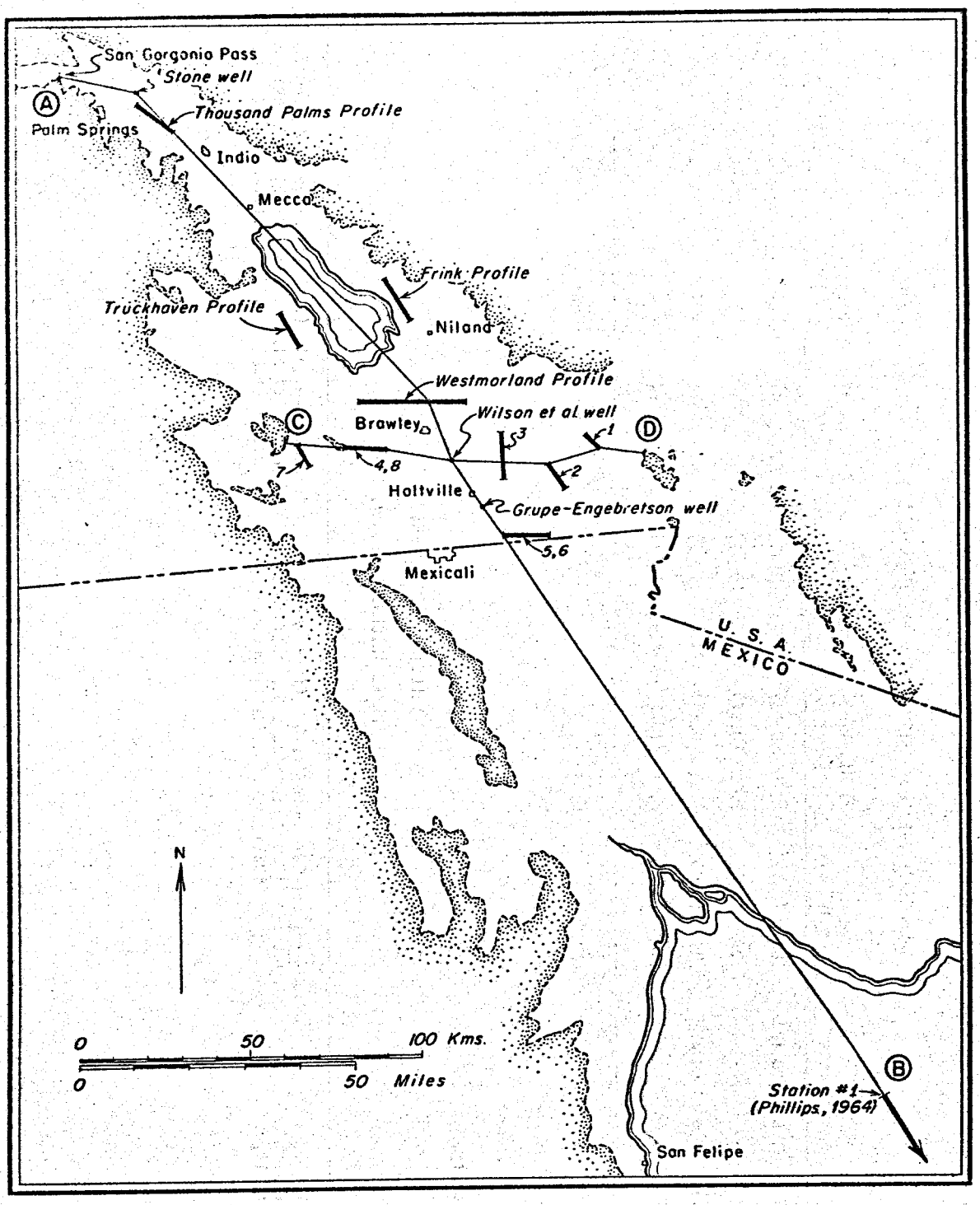

Figure 2

Index Map showing location of previous refraction profiles in the Imperial Valley (after Biehler, 1964). Letters (A)-(B) and (C)-(D) denote seismic cross-section lines used by Biehler. The number 1-8 denote seismic profiles: 1-Glamis-Ogilby, 2-Coachella Canal, 3-East Highline Canal, 4,8-Superstition Hills, 5,6-Mexican Border, 7-Plaster City.

TABLE 1

SUMMARY OF PREVIOUS SEISMIC VELOCITY INFORMATION OF THE IMPERIAL VALLEY

Westmoreland[1]		Truckhaven[2]		Frink[3]		E. Highline Canal[4]		Mexican Border[5]		Coachella Canal[6]		Plaster City[7]		Glamis-Ogilby[8]		Superstition Hills[9]	
1.70	(0.18)	1.67	(0.12)	1.85	(0.15)	1.75	(0.43)	1.85	(0.49)	1.91	(0.4)	----	-----	----	------	1.72	(0.21)
1.96	(0.55)	----	------	2.07	(0.46)	2.32	(0.97)	2.31	(0.51)	2.22	(0.44)	2.11	(0.8)	2.12	(0.55)	2.13	(0.35)
2.71	(0.975)	2.32	(0.26)	3.04	(0.43)	2.62	(0.26)	2.60	(1.19)	2.67	(0.75)	----	-----	----	------	2.41	(1.20)
3.76	(1.19)	3.69	(0.73)	4.20	(1.19)	3.81	(1.42)	3.63	(1.37)	3.37	(1.24)	----	-----	----	------	3.26	(1.00)
4.70	(2.68)	----	------	----	------	----	------	4.72		----	------	----	-----	----	------	4.33	------
6.40*		5.38*		5.39*		5.5*				6.1*		5.86*		5.64*			

*Basement velocity.

VELOCITIES IN KM/SEC.

(LAYER THICKNESS) IN KM.

1. Biehler (1964).
2. Biehler (1964).
3. Biehler (1964).
4. Kovach et al. (1962), profile 3., figure 2.
5. Kovach et al. (1962), profiles 5,6., figure 2.
6. Kovach et al. (1962), profile 2., figure 2.
7. Kovach et al. (1962), profile 7, figure 2.
8. Kovach et al. (1962), profile 1, figure 2.
9. Kovach et al. (1962), profiles 4,8, figure 2.

REFRACTION INSTRUMENTATION AND FIELD METHODS

To investigate the sedimentary section and basement depth within the geothermal area, seven seismic refraction profiles were shot (Figure 3). Shot points were chosen for ease of accessibility and strategic location within the geothermal area. The northern section of the geothermal field was inaccessible due to flooding and agricultural activity. The profile lines were chosen to provide maximum interrogation of the geothermal area, and also to augment information from previous seismic refraction studies to the east and south (Biehler, 1964). Four additional long-distance refraction shots were used to investigate areas adjacent the geothermal area. A summary of shot-point and profile information is contained in Table 2.

The seismic profiles were shot keeping the shot-points fixed and moving the detector spread progressively outward. Six of the profiles were reversed. The profile lines intersect at several points (Figure 3), thus interrogating the same approximate areas. This provides a check on depth calculations.

Two seismic refraction systems were employed in collecting the seismic data, with both systems recording each shot. The primary system consisted of two Dresser SIE portable 12-channel amplifiers and a 24-channel recording oscillograph, used in conjunction with 24 8hz geophones. The primary system detector spread-length was 1400 meters, with an individual geophone spacing of 61 meters. The secondary system was a 12-channel amplifier-recorder, with 12 8hz geophones. The spread-length was 335 meters, with a

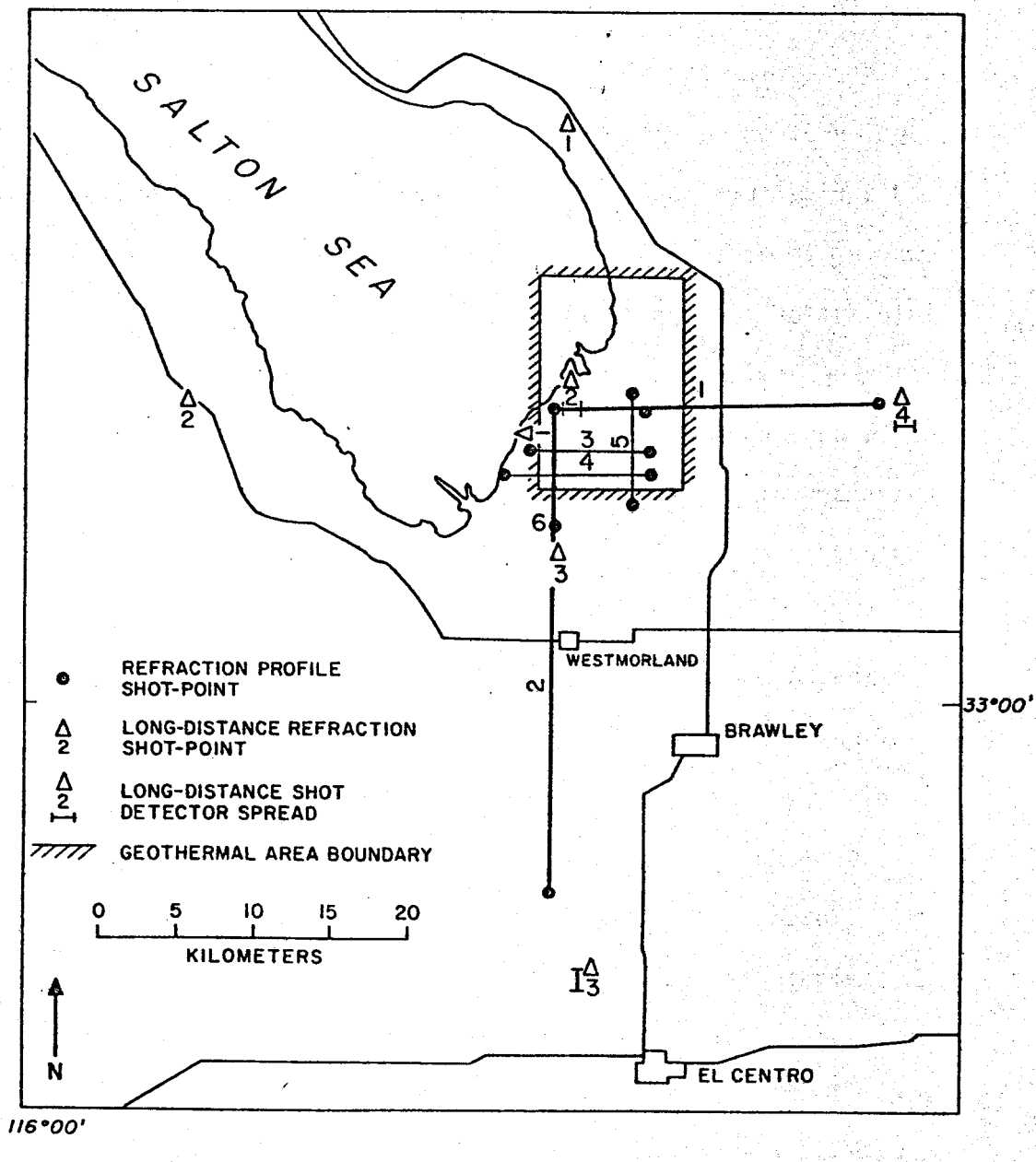

Figure 3
Index map showing locations of refraction profiles and long-distance refraction shot-points.

TABLE 2

SUMMARY OF SHOT-POINT LOCATIONS

Profile	Length (km)	Shot-Point Location	
		Forward	Reverse
1	20.7	Obsidian Butte (33°10.16'N. LAT, 115°37.9'W. LONG)	East Highline Canal at Sinclair Road (33°10.57'N. LAT, 115°24.7'W. LONG)
1*	5.8	Obsidian Butte (33°10.15'N. LAT, 115°37.9'W. LONG)	Alamo River at McKendry Road (33°10.2'N. LAT, 115°34.2'W. LONG)
2	30.8	Obsidian Butte (33°10.16'N. LAT, 115°37.9'W. LONG)	Westside Canal (32°53.4'N. LAT, 115°38.03' W. LONG)
3	7.5	I.I.D. Vail Lateral 6 at Lindsay Road (33°8.85'N. LAT, 115°38.9'W. LONG)	Alamo River at Lindsay Road (33°8.85'N. LAT, 115°34.06'W. LONG)
4	9.2	I.I.D. Vail Lateral 7 at Young Road (33°7.9'N. LAT, 115°39.9'W. LONG)	Alamo River at Young Road (33°7.9'N. LAT, 115°33.97'W. LONG)
5	6.9	Alamo River (33°10.8'N. LAT, 115°34.75'W. LONG)	Intersection of Kalin Road and Bowles Road (33°7.07'N. LAT, 115°34.57'W. LONG)
6	7	I.I.D. Vail Lateral 5 at Severe Road (33°6.25'N. LAT, 115°37.8'W. LONG)	
Shot 1	18†	State Highway 111 near Frink Spring (33°20.3'N. LAT, 115°37.7'W. LONG)	
Shot 2	24.3†	Entry to Salton Sea Test Base Road (33°10.6'N. LAT, 115°53.4'W. LONG)	
Shot 3	28.3†	New River at Severe Road (33°5.2'N. LAT, 115°37.8'W. LONG)	
Shot 4	22.4†	Obsidian Butte (33°10.16'N. LAT, 115°37.9'W. LONG)	

†Distance from shot-point to first geophone.

geophone spacing of 30.5 meters

Shot holes were drilled to depths between 10 and 16 meters. Explosive charge sizes ranged from 4.5 kg to 67.5 kg of DuPont 60% high velocity seismic gel. For long-distance shot 3, 900 kg of DuPont Pourvex Extra was used, with 300 kg in three 15 meters holes.

The seismic data were collected between April and December, 1975, with the aid of student volunteers and employees of the Institute of Geophysics and Planetary Physics from the University of California at Riverside.

REFRACTION PROFILE DESCRIPTIONS

First arrivals and all major secondary arrivals are presented in conventional time-distance plots. Most first arrivals could easily be read to ± 0.02 sec. Weak arrivals and any unusual behavior in first energy are discussed in the text of individual profiles. Examples of the refraction arrivals are presented in Figure 4.

The flat topography of the survey area and use of shallow shot hole depths made elevation corrections unnecessary.

Profile 1

This profile (shown in Figure 5) was not reversed in the conventional sense. The reverse profile was shot 0.8 km north of the forward profile because of the lack of acceptable shot-point locations along the line of the forward profile. For purposes of interpretation, the data are presented in a reverse-profile format.

Arrivals of 0.35 km/sec occurred as easily read secondary events. These arrivals were observed in only one short-distance recording in the forward direction (Figure 6). The apparent absence of these arrivals from other recordings is most likely the result of background noise generated by frequent agricultural activity concealing their presence. For interpretive purposes, arrivals of 0.35 km/sec are assumed present in the reverse direction (denoted by a dashed line in Figure 5).

First arrivals of 1.70 km/sec were easily read in recordings from both forward and reverse directions. Emergent secondary arrivals

FIGURE 4

Representative tracing of recorded arrivals

(A) easily read arrivals

(B) weak and noisy arrivals

(C) weak arrivals, with emergent secondary peaks.

Tic marks (') indicate interpreted first breaks, and (^) secondary arrivals.

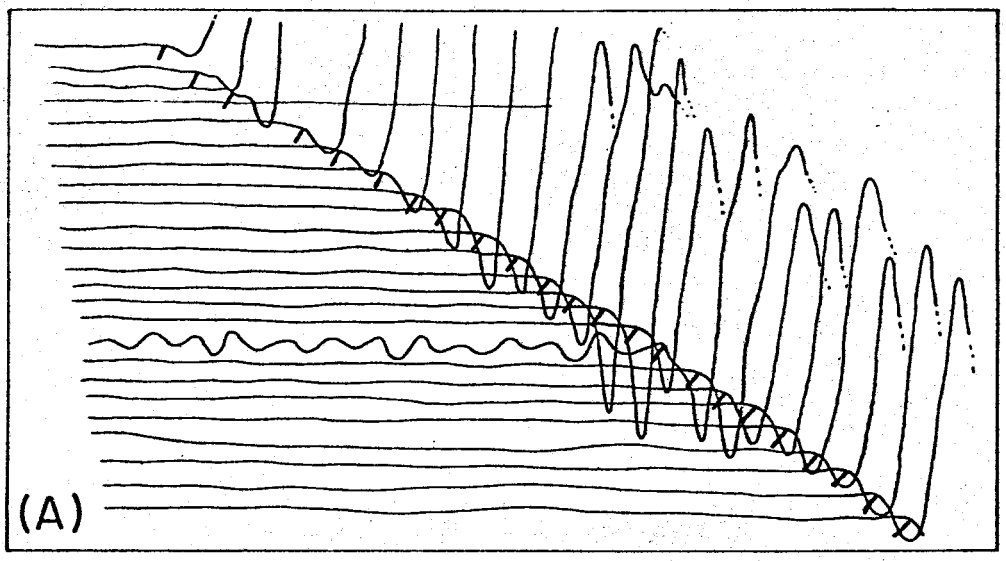
(A)

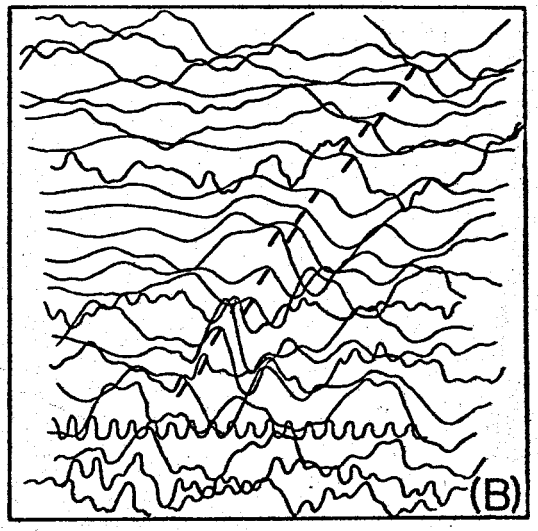
(B)

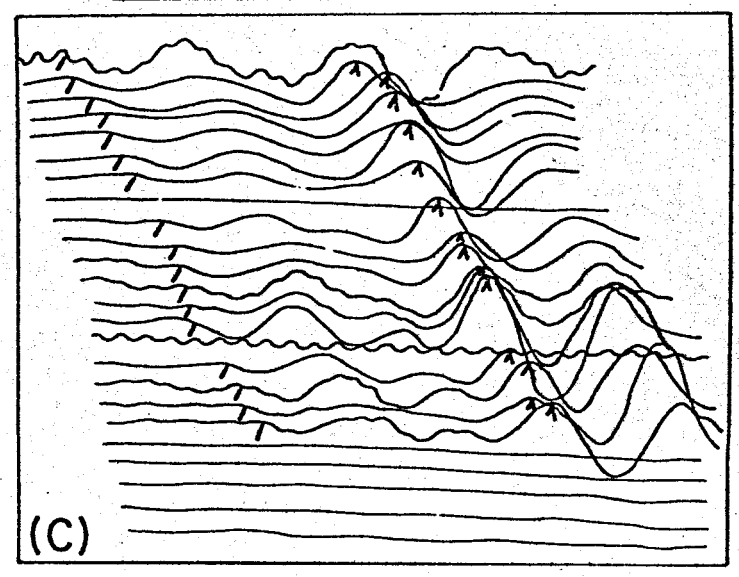
(C)

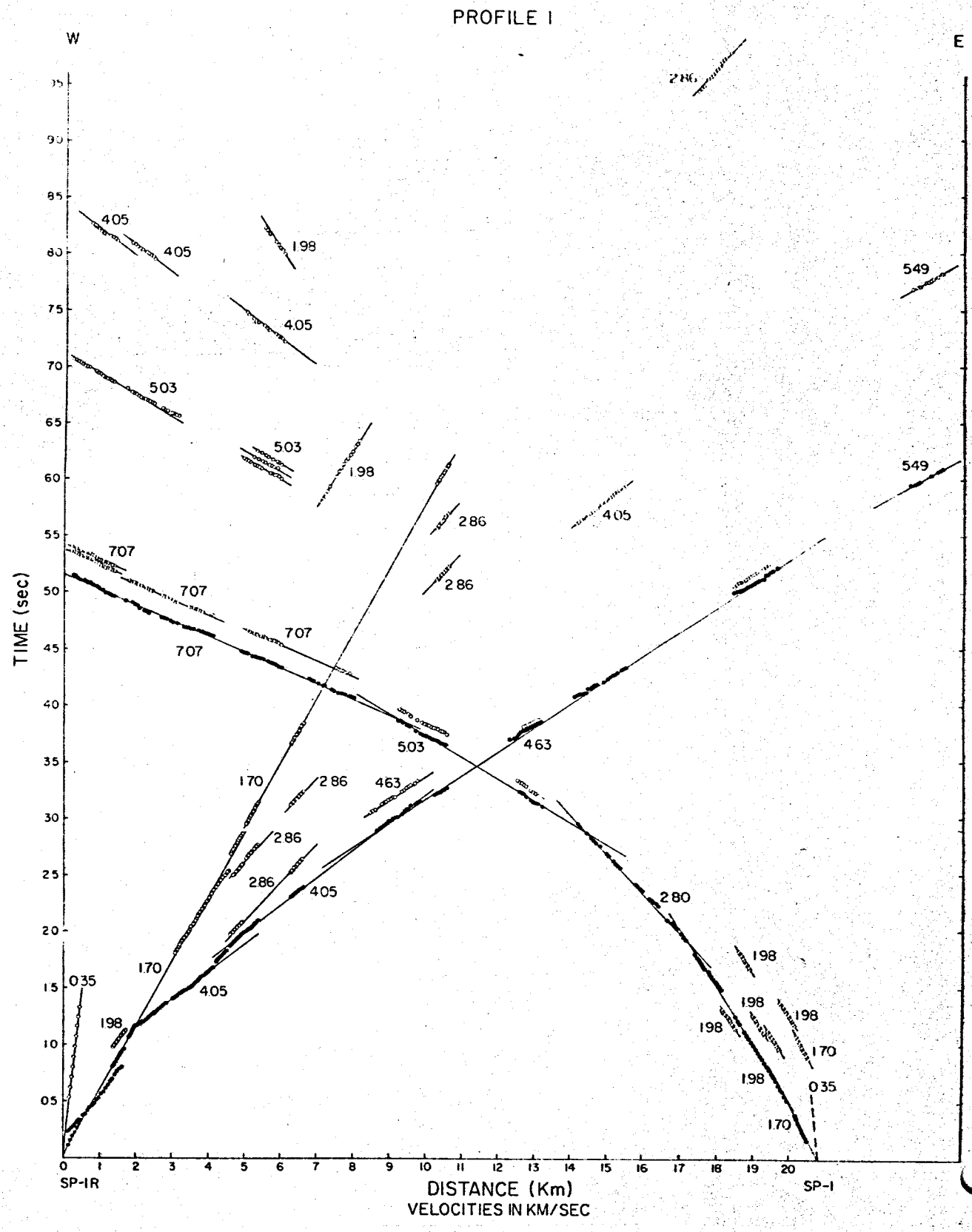

Figure 5
Time-Distance Plot of Profile 1

First arrivals are plotted as solid circles; later arrivals are

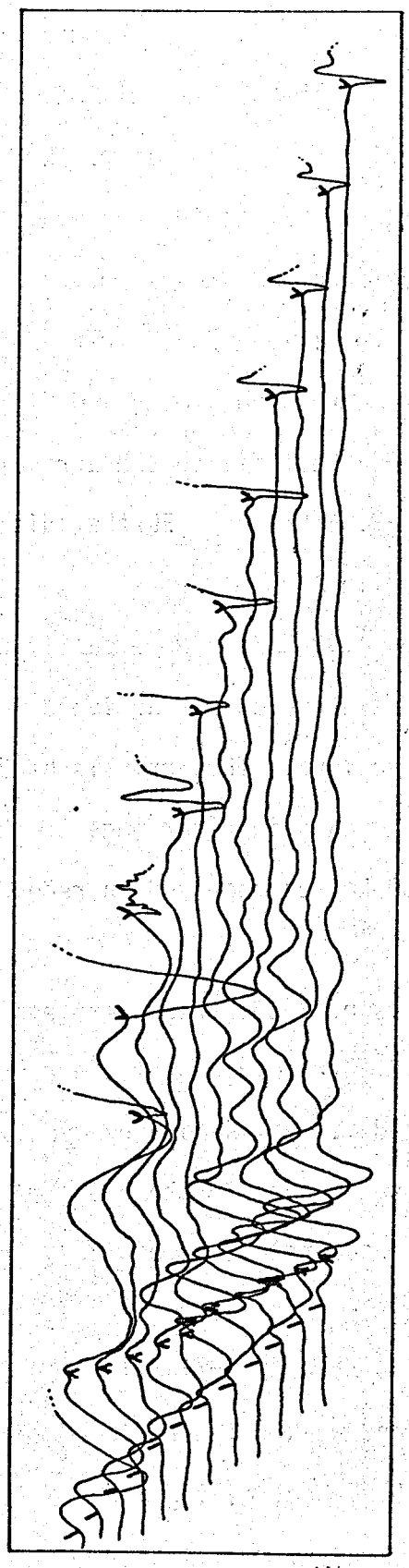

Figure 6

Representative tracing of refraction recording with 1.70 km/sec first arrivals, represented by tic marks ('); interpreted reflection arrivals represented by ^; arrivals of 0.35 km/sec, represented by V.

occurred in recordings of the forward direction. A reflection occurs in the 1.70 km/sec arrivals recorded at 0.5 km (Figure 6). A calculation assuming a horizontal reflecting interface and a two-way travel time of 0.2 sec yields a depth of 0.17 km. A departure from a linear fit occurs at 1 km in the 1.70 km/sec first arrivals in the forward direction (Figure 5). Errors in timing and field procedure can be eliminated. Obtaining a best fit to the arrivals showing the departure yielded a velocity of 2.86 km/sec. Further discussion is given in the interpretation of Profile 1.

First arrivals of 1.98 km/sec were easily read in recordings of the reverse profile. Emergent secondary arrivals were observed in recordings from both profile directions. The arrivals of 2.86 km/sec were observed as emergent secondary events in recordings of the forward direction. First arrivals of 2.80 km/sec observed in recordings of the reverse direction were weak.

The first arrivals of 4.05 km/sec were easily read in the forward direction recordings. In recordings of the reverse direction, arrivals of 4.05 km/sec occurred as weak secondary events. At 4.5 km an offset of approximately 0.1 sec occurs in the 4.05 km/sec first arrivals (Figure 5), which is interpreted as resulting from a fault with a throw of 215 meters.

The first arrivals of 4.63 km/sec in recordings of the forward direction were noisy and weak (Figure 7). Uncertainties in first arrival times were $\pm$ 0.05 sec, giving a range in interpreted apparent velocity of $\pm$ 10%. Secondary arrivals aided in establishing the apparent velocity. First arrivals of 5.03 km/sec were easily read in recordings

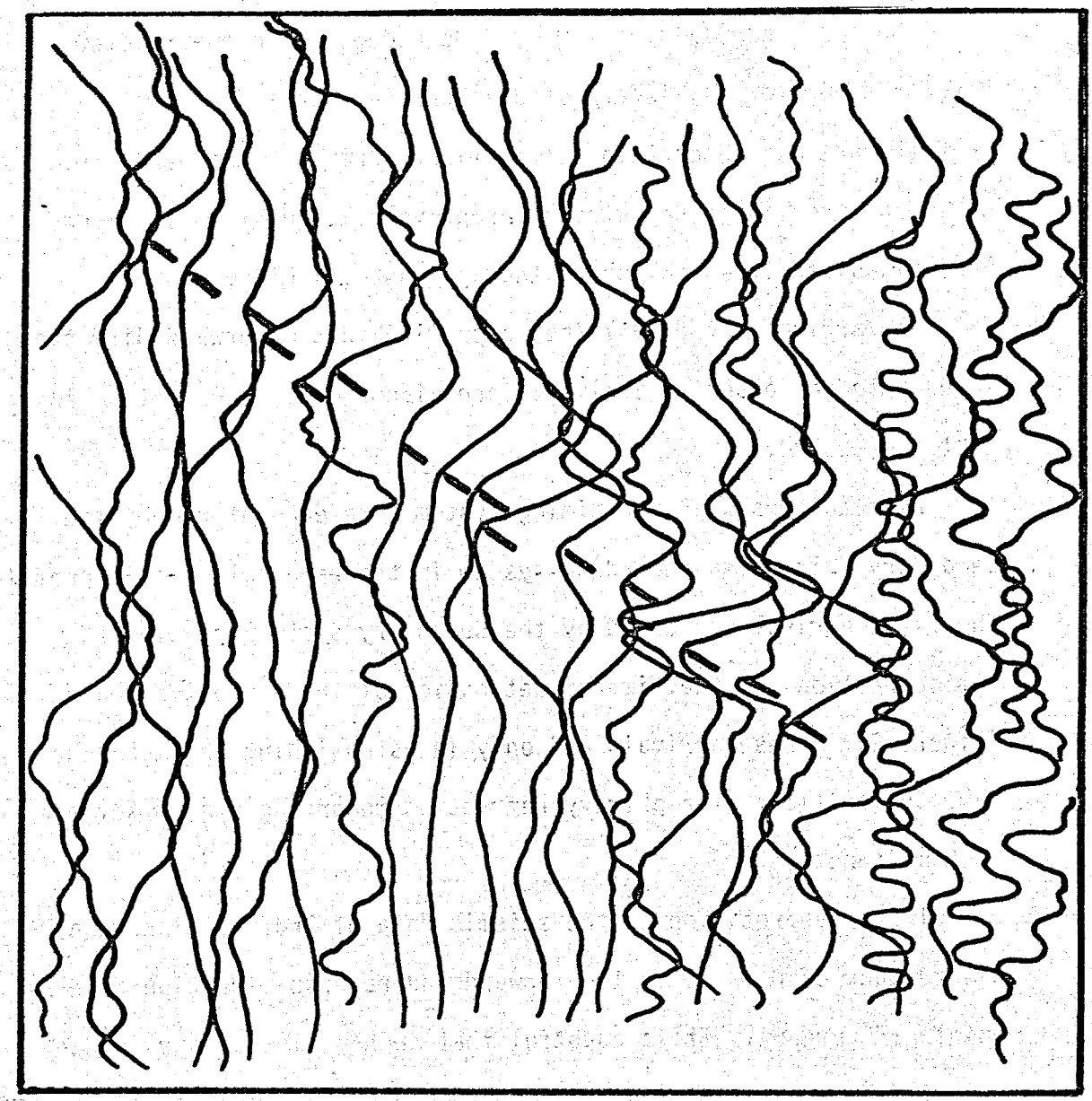

Figure 7

Representative tracing of refraction recording with weak and noisy first arrivals of 4.63 km/sec. Interpreted first breaks are indicated by tic marks (').

of the reverse direction. The difference in forward (4.63 km/sec) and reverse (5.03 km/sec) apparent velocities indicates an easterly dip on the order of 3 to 5 degrees.

The first arrivals of 7.07 km/sec occurring in the reverse direction recordings, interpreted as basement arrivals, were noisy and weak (Figure 8). Uncertainties in first arrival times were $\pm$ 0.05 sec, giving a range in interpreted apparent velocity of $\pm$ 10%. Secondary arrivals aided in establishing the apparent velocity.

The arrivals of 5.49 km/sec occurring in the forward direction, interpreted as basement arrivals, are discussed in the text of long-distance shot 4.

Difficulties with the timing system were encountered by the secondary refraction recording system in the reversal of this profile. The first arrivals recorded by the secondary system are plotted without correction for the time of detonation of the explosive charge (Figure 5). These arrivals aid only in establishing the apparent layer velocities. The primary refraction recording system suffered no such malfunction.

The interpretation of the seismic data of Profile 1 shows a discrepancy of 0.3 sec in the forward and reverse direction reverse points (Figure 5). It is doubtful that such a discrepancy is due only to the 0.8 km between the forward and reverse profile lines. The possibility of missing seismic layers due to weak first energy arrivals is also doubtful, as seismic layer velocities obtained from sites to the east and north (Biehler, 1964) agree well with the interpreted seismic velocities in Profile 1. A remaining alternative to the reverse-

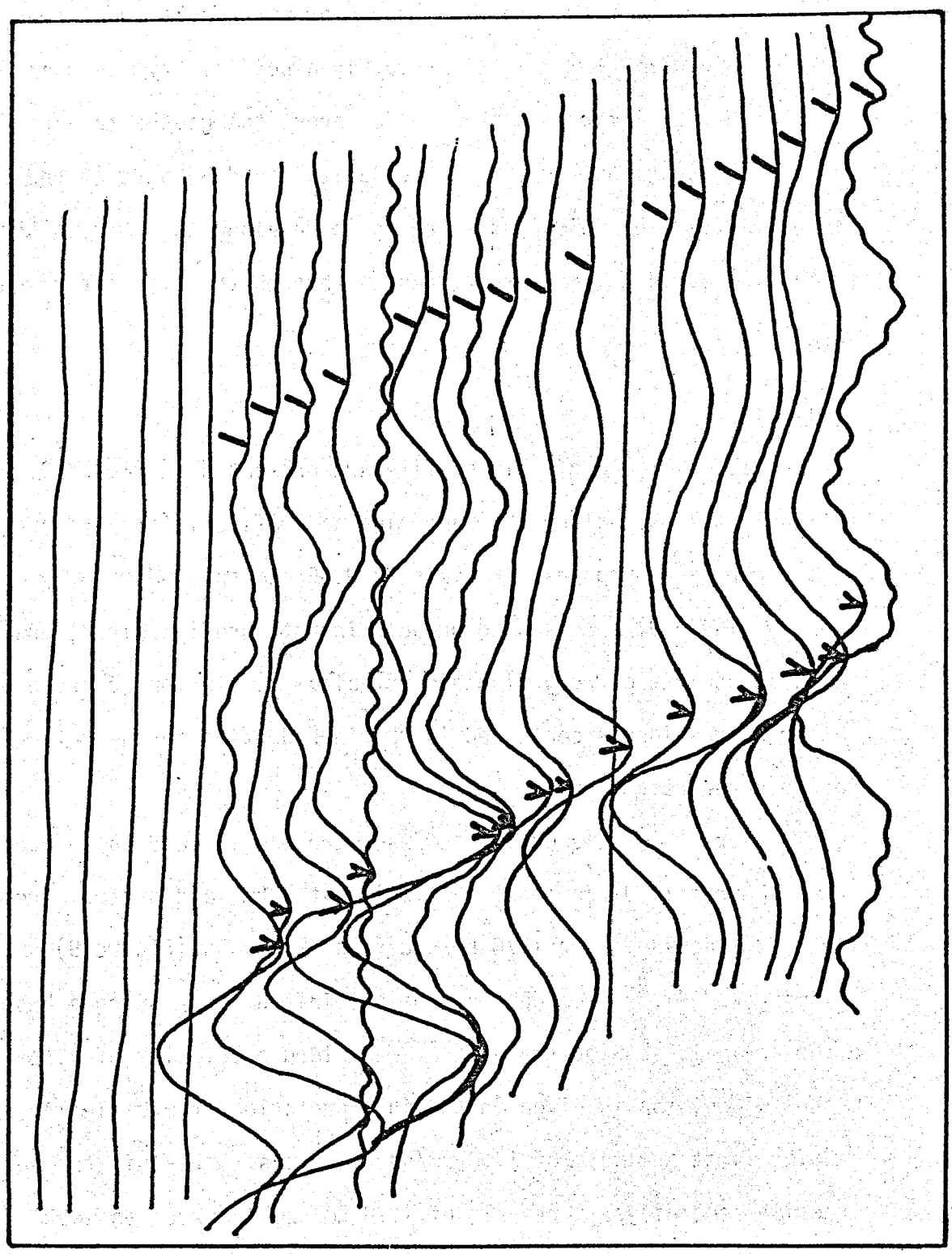

Figure 8

Representative tracing of refraction recording with weak and noisy first arrivals of 7.07 km/sec. Interpreted first breaks are indicated by the tic marks ('). An emergent secondary peak is indicated by ^.

point discrepancy is the crossing of one or more fault zones not detected in Profile 1. This is certainly a possibility, as numerous faults have been inferred within and adjacent the geothermal area (compiled by Jennings, 1975). These faults could be part of the San Andreas fault zone, which, if extended south along the eastern shore of the Salton Sea (Jennings, 1967), passes through the area interrogated by Profile 1.

Profile 1*

The seismic data of this profile are presented in Figure 9. Profile 1* was shot along the same line as Profile 1 (forward profile). For interpretive purposes, arrivals of 0.35 km/sec, denoted by dashed lines in Figure 9, are assumed present in both profile directions. The duration time of recording did not allow resolution of these arrivals. Further discussion is contained in the introduction to the refraction profile interpretations.

The first arrivals of 1.70 km/sec were easily read in recordings from both profile directions. Beginning at 1 km, a departure from a linear fit occurs in the 1.70 km/sec first arrivals (Figure 9). Errors in timing and field procedure can be eliminated. Obtaining a best fit to the arrivals showing the departure yielded a velocity of 2.86 km/sec. Further discussion is given in the interpretation of Profile 1*.

The first arrivals of 1.98 km/sec were easily read in the reverse direction recordings. Arrivals of 1.98 km/sec occurred as weak secondary events in the forward direction.

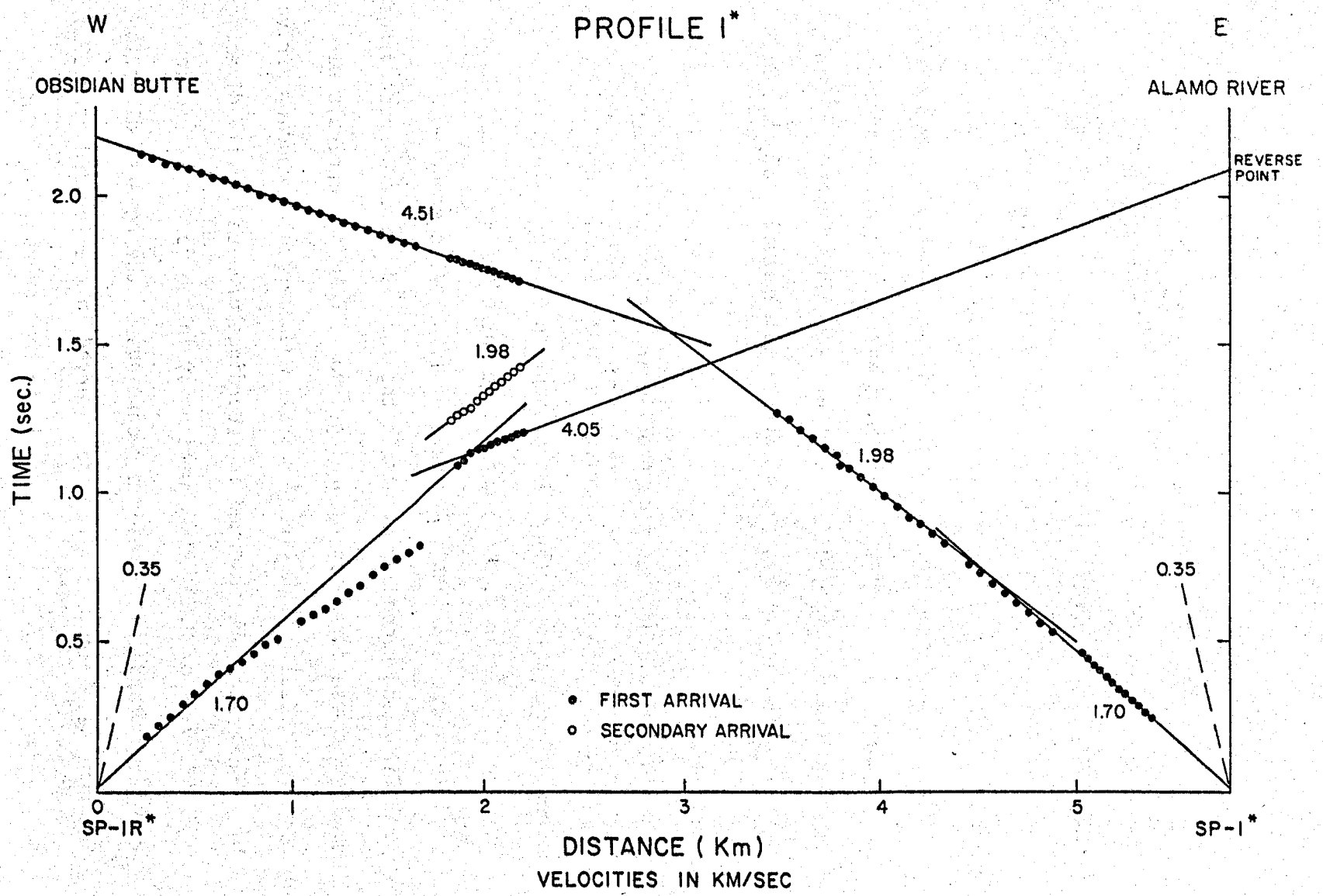

Figure 9

Time-Distance Plot of Profile 1*.

First arrivals of 4.05 km/sec were easily read in the forward directions. No 4.05 km/sec arrivals were observed in the reverse direction recordings. Easily read first arrivals of 4.51 km/sec were observed in the forward direction.

Extrapolating the 4.05 km/sec arrivals to a reverse point and comparing with the reverse point obtained from the 4.51 km/sec arrivals, yielded a discrepancy of 0.1 sec. This descrepancy was explained by an obscure 0.1 sec offset in the 4.05 km/sec arrivals produced by the fault detected in Profile 1. Lack of recordings beyond 2 km in the forward direction of Profile 1* prevented resolution of this fault.

Profile 2

The seismic data of this profile are presented in Figure 10. For interpretive purposes, arrivals of 0.35 km/sec, denoted by dashed lines in Figure 10, are assumed present in both profile directions. Further discussion is contained in the introduction to the refraction profile interpretations. Arrivals of 1.70 km/sec occurred as easily read first and secondary events in the forward direction recordings. In the reverse direction recordings, no 1.70 km/sec arrivals were observed. Easily read first arrivals and emergent secondary arrivals of 1.95 km/sec were observed in recordings of both profile directions.

Arrivals of 2.80 km/sec were noisy in the forward direction recordings, and easily read in recordings of the reverse direction. Emergent secondary arrivals were observed in the forward direction recordings and 3.72 km/sec arrivals in the reverse direction recordings were easily read.

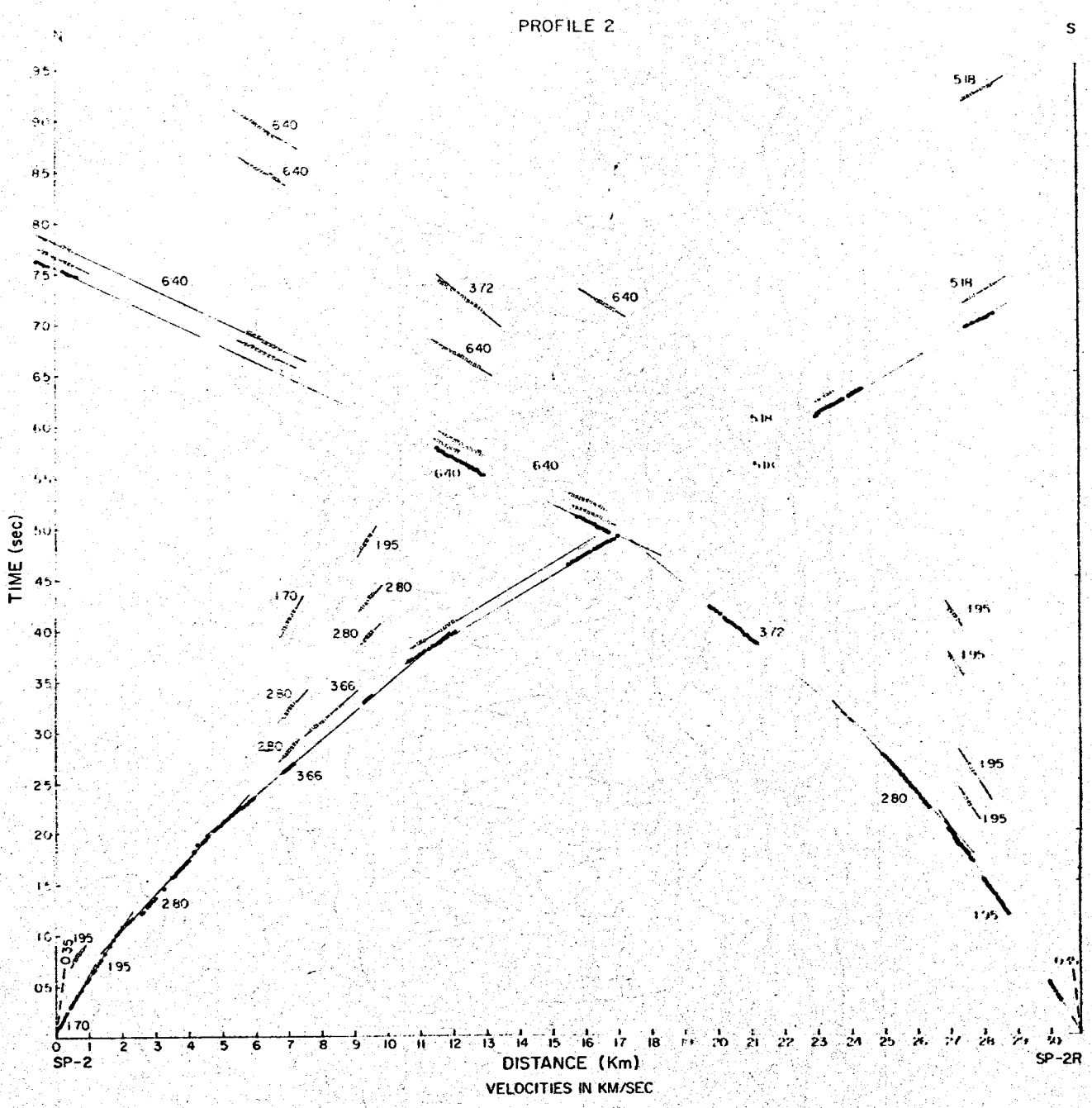

Figure 10

Time-Distance Plot of Profile 2. First arrivals are plotted as solid circles; later arrivals are plotted as open circles.

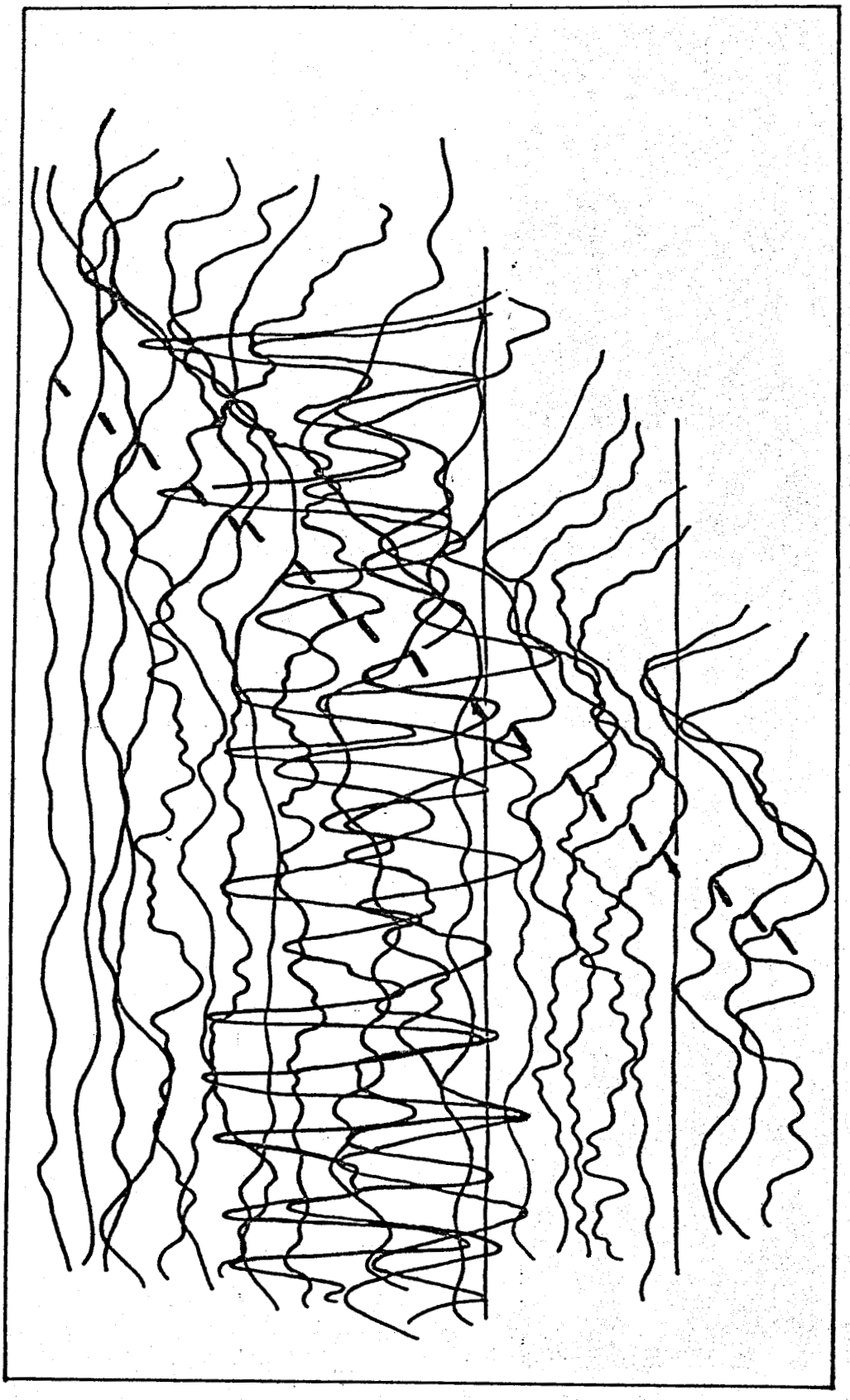

Figure 11

Representative tracing of refraction recording with noisy first arrivals of 5.18 km/sec. Interpreted first breaks are indicated by tic marks (').

The first arrivals of 5.18 km/sec in the recordings of the forward direction were noisy (Figure 11). Uncertainties in first arrival times were ± 0.05 sec, giving a range in interpreted apparent velocity of ± 10%. Secondary arrivals aided in establishing the apparent velocity. The 5.18 km/sec arrivals are not interpreted as basement events, as the signature of the first arrivals exhibits a high frequency content that is not consistent with basement arrivals (personal communication, Biehler, 1978). A discussion of frequency content and seismic layer interpretation is contained in Dohr (1974). Arrivals of 5.18 km/sec were not observed in the reverse direction.

The first arrivals of 6.40 km/sec in the reverse direction recordings were noisy and weak. Uncertainties in first arrival times were ± 0.05 sec, giving a range in interpreted apparent velocity of ± 10%. Secondary arrivals aided in establishing the apparent velocity. The 6.40 km/sec arrivals are interpreted as basement events. No basement arrivals were observed in the forward direction recordings.

Profile 3

The seismic data of this profile are presented in Figure 12. For interpretive purposes, arrivals of 0.35 km/sec, denoted by dashed lines in Figure 12, are assumed present in both profile directions. Further discussion is contained in the introduction to the refraction profile interpretations. First arrivals of 1.70 km/sec in the reverse direction recordings were weak. Emergent secondary arrivals of 1.70 km/sec occurred in the forward direction. Arrivals showing an apparent departure from linearity begin at 1 km. Errors in timing and field

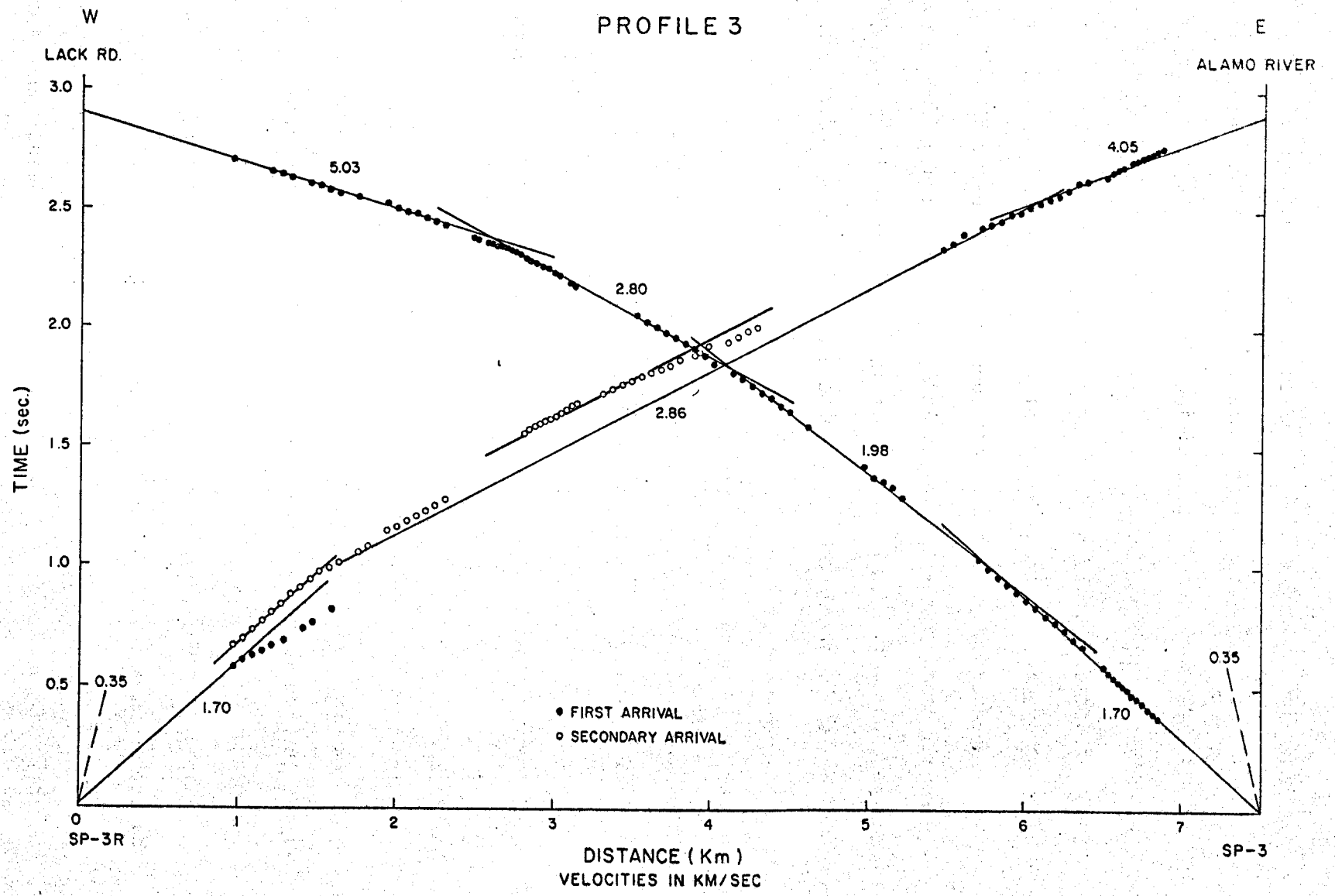

Figure 12

Time-Distance Plot of Profile 3.

procedure can be eliminated. Obtaining a best fit to the arrivals showing the departure yielded a velocity of 2.86 km/sec. Further discussion is given in the interpretation of Profile 3.

Noisy first arrivals of 2.80 km/sec were observed in the reverse direction recordings. The secondary arrivals of 2.86 km/sec in the forward direction were weak and noisy.

The first arrivals of 4.05 km/sec were easily read in recordings of the forward direction. Arrivals of 4.05 km/sec were not observed in the reverse direction recordings. Easily read first arrivals of 5.03 km/sec occurred in the reverse direction recordings. Arrivals of 5.03 km/sec were not observed in the recordings of the forward direction.

Due to logistical problems, no recordings were made between 4.5 and 5.5 km in the reversed profile.

Profile 4

The seismic data of this profile are presented in Figure 13. For interpretive purposes, arrivals of 0.35 km/sec, denoted by dashed lines in Figure 13, are assumed present in both profile directions. Further discussion is contained in the introduction to the refraction profile interpretations. First arrivals of 1.70 km/sec were easily read in the reverse direction recordings. Emergent secondary arrivals occurred in the recordings of both profile directions. First arrivals of 1.98 km/sec were easily read in the recordings of the reverse direction recordings.

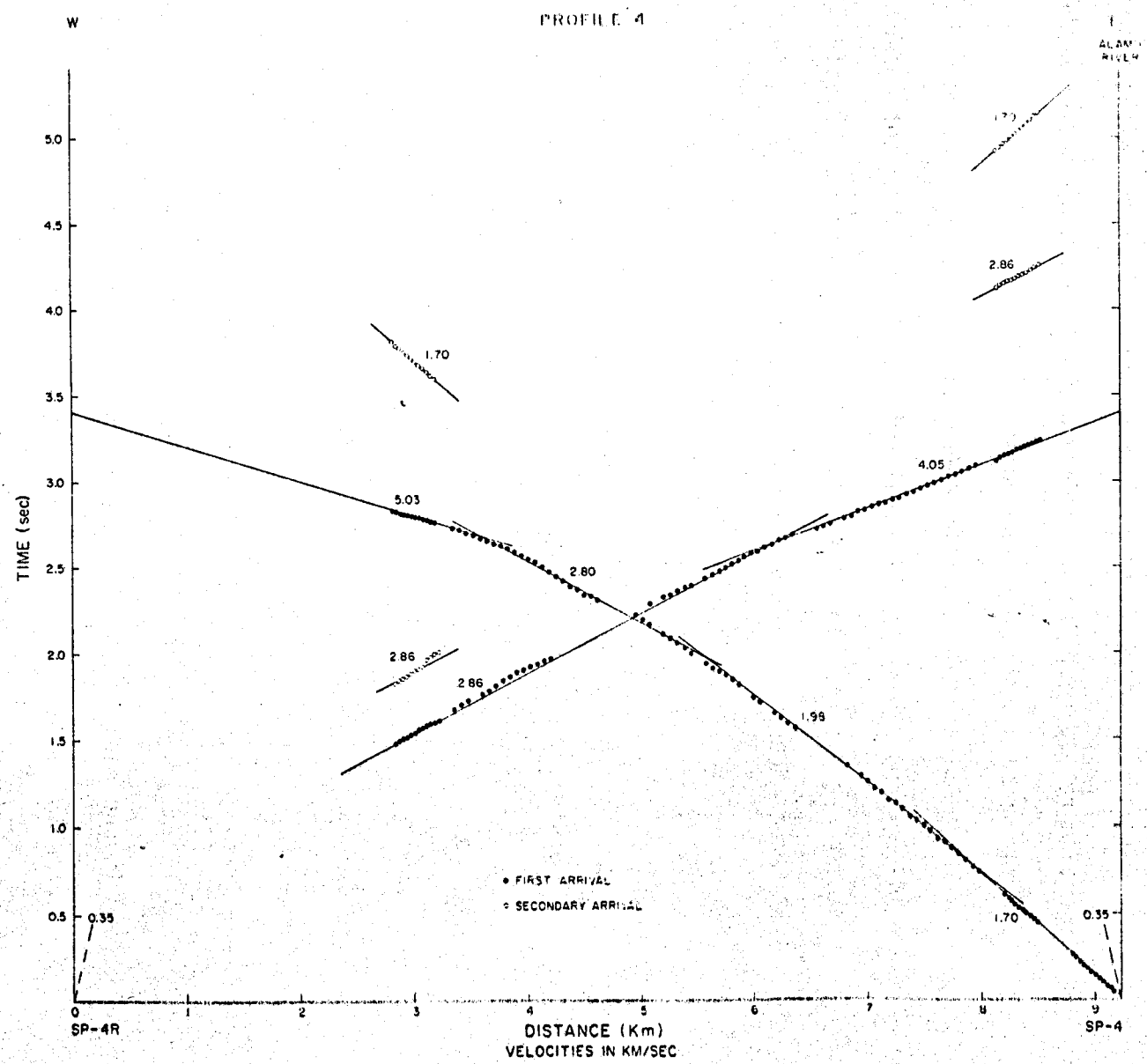

Figure 13

Time-Distance Plot of Spread 4.

The first arrivals of 2.86 km/sec in the forward direction recordings were noisy. Departures from a linear fit are attributed to uncertainties in first arrival times (± 0.04 sec). Emergent secondary arrivals were observed in the forward direction recordings. First arrivals of 2.80 km/sec in the reverse direction recordings were easily read.

The first arrivals of 4.05 km/sec in the forward direction recordings were easily read. Arrivals of 4.05 km/sec were not observed in the reverse direction recordings. Easily read first arrivals of 5.03 km/sec occurred in the reverse direction recordings. Arrivals of 5.03 km/sec were not observed in recordings of the forward direction.

Logistical problems prevented recordings between the zero-point and 3 km.

Profile 5

The seismic data of this profile are presented in Figure 14. For interpretive purposes, arrivals of 0.35 km/sec, denoted by dashed lines in Figure 14, are assumed present in both profile directions. Further discussion is contained in the introduction to the refraction profile interpretations. The first arrivals of 1.70 km/sec in the reverse direction recordings were easily read. Arrivals of 1.70 km/sec in the forward direction recordings occurred as emergent secondary events. First arrivals of 1.95 and 2.80 km/sec were easily read in the recordings of both profile directions. Emergent secondary arrivals of 2.80 km/sec occurred in the forward direction recordings. In the reverse direction first arrivals of 2.80 km/sec show an offset of

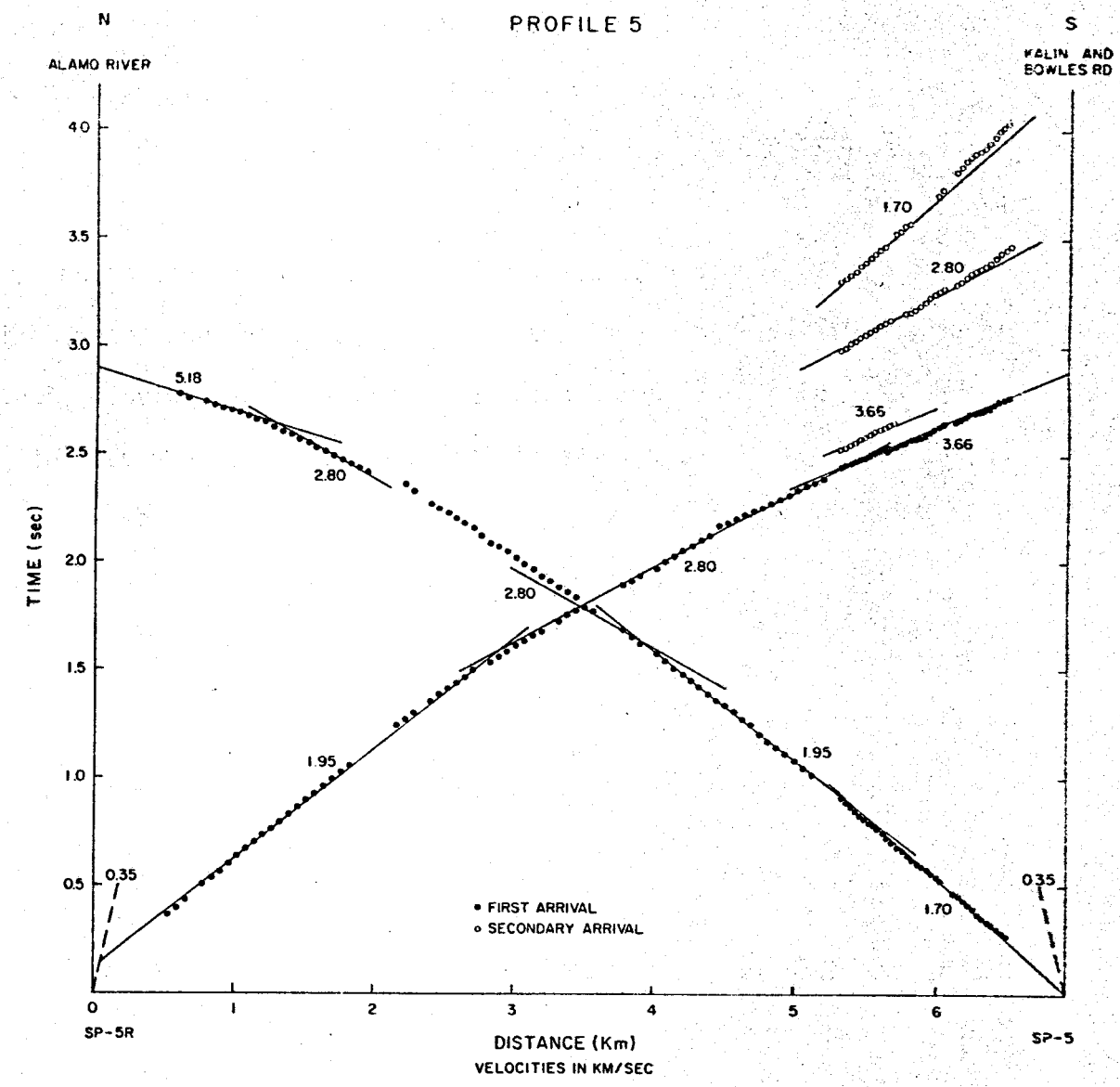

Figure 14

Time-Distance Plot of Profile 5.

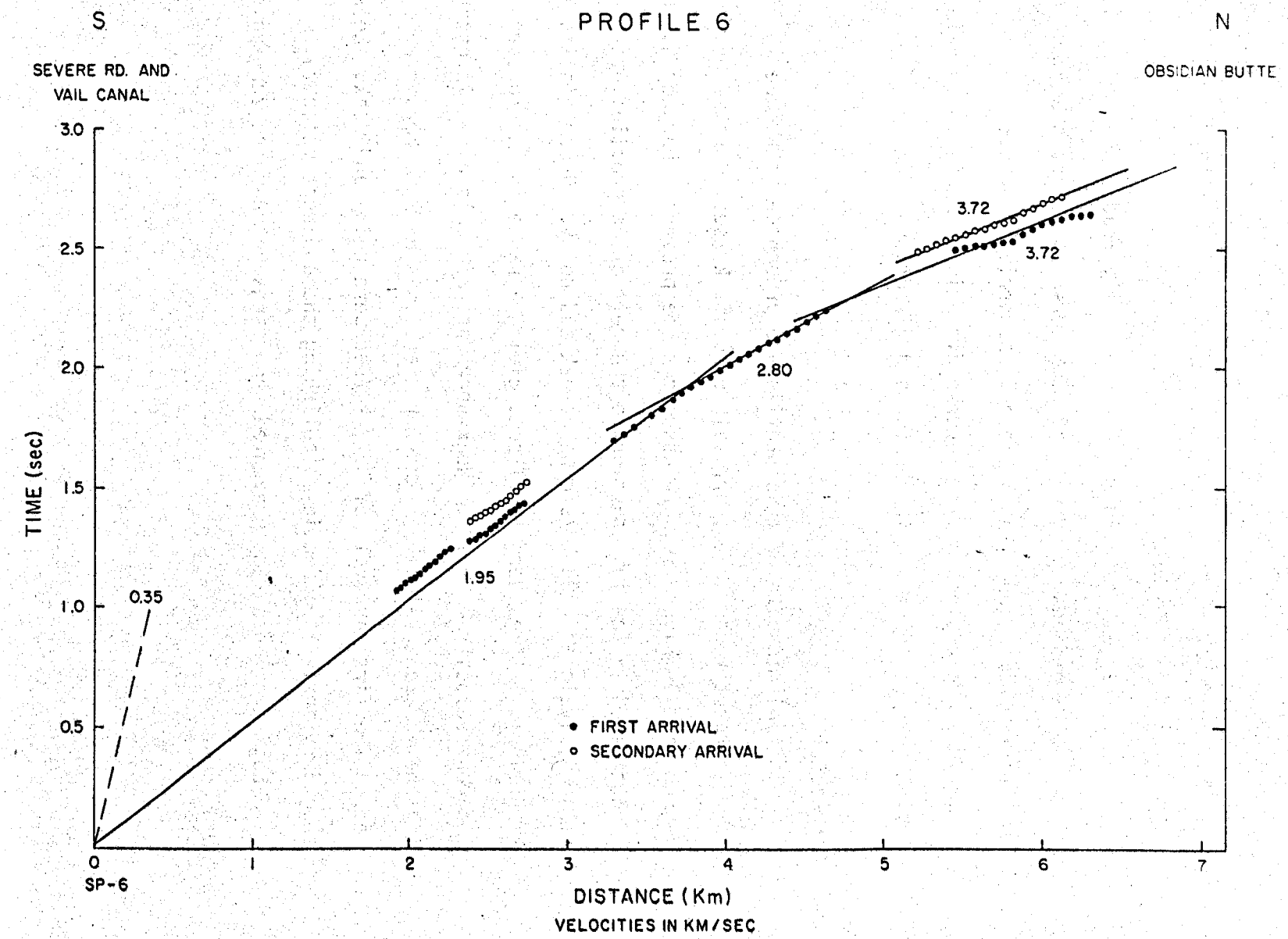

Figure 15

Time-Distance Plot of Profile 6.

approximately 0.07 sec, which is interpreted as resulting from a fault with a throw of 100 meters.

First arrivals of 3.66 km/sec were easily read in the forward direction recordings. Arrivals of 3.66 km/sec were not observed in the reverse direction. Easily read first arrivals of 5.18 km/sec occurred in recordings of the reverse direction. Arrivals of 5.18 km/sec were not observed in the forward direction.

Profile 6

The seismic data of this profile are presented in Figure 15. For interpretive purposes, arrivals of 0.35 km/sec, denoted by a dashed line in Figure 15, are assumed to be present. Further discussion is contained in the introduction to the refraction profile interpretations. First arrivals of 1.95 km/sec were weak and noisy. Uncertainties in first arrival times were $\pm$ 0.1 sec, giving a range in interpreted apparent velocity of $\pm$ 10%. Weak secondary arrivals aided in establishing the apparent velocity. The first arrivals of 2.80 km/sec were easily read. The first arrivals of 3.72 km/sec were noisy and weak. Noisy secondary arrivals aided in establishing the apparent velocity.

Logistical problems prevented recordings between the zero-point and 2 km.

LONG-DISTANCE REFRACTION SHOT DESCRIPTIONS

Shot 1

Arrivals from this shot are presented in Figure 16. First arrivals could not be read accurately due to high background noise. Secondary arrivals of 6.57 and 5.03 km/sec were weak. The 6.57 km/sec arrivals are interpreted as basement events.

The apparent basement velocity obtained in Shot 1 (6.57 km/sec) is in close agreement with that obtained in Profile 2 (6.40 km/sec). The 5.03 km/sec velocity is in close agreement with the apparent seismic velocities reported in Profiles 1, 2, 3, 4 and 5 (5.03 km/sec in Profiles 1, 3 and 4; 5.18 km/sec in Profiles 2 and 5).

Shot 2

Arrivals from this shot are presented in Figure 16. First arrivals could not be read accurately due to high background noise. Secondary arrivals of 5.27 km/sec were easily read. Based on their low-frequency signature, the 5.27 km/sec arrivals are interpreted as basement events. A discussion of frequency content and seismic layer interpretation is contained in Dohr (1974). Emergent secondary arrivals of 4.05 and 2.86 km/sec were observed. The 2.86 and 4.05 km/sec velocities are in exact agreement with the apparent seismic velocities reported in Profiles 1, 3 and 4.

Shot 3

First and secondary arrivals are presented in Figure 16. The first arrivals of 5.77 km/sec were easily read. Emergent secondary arrivals of 5.77, 3.16, 2.80 and 1.95 km/sec were also observed.

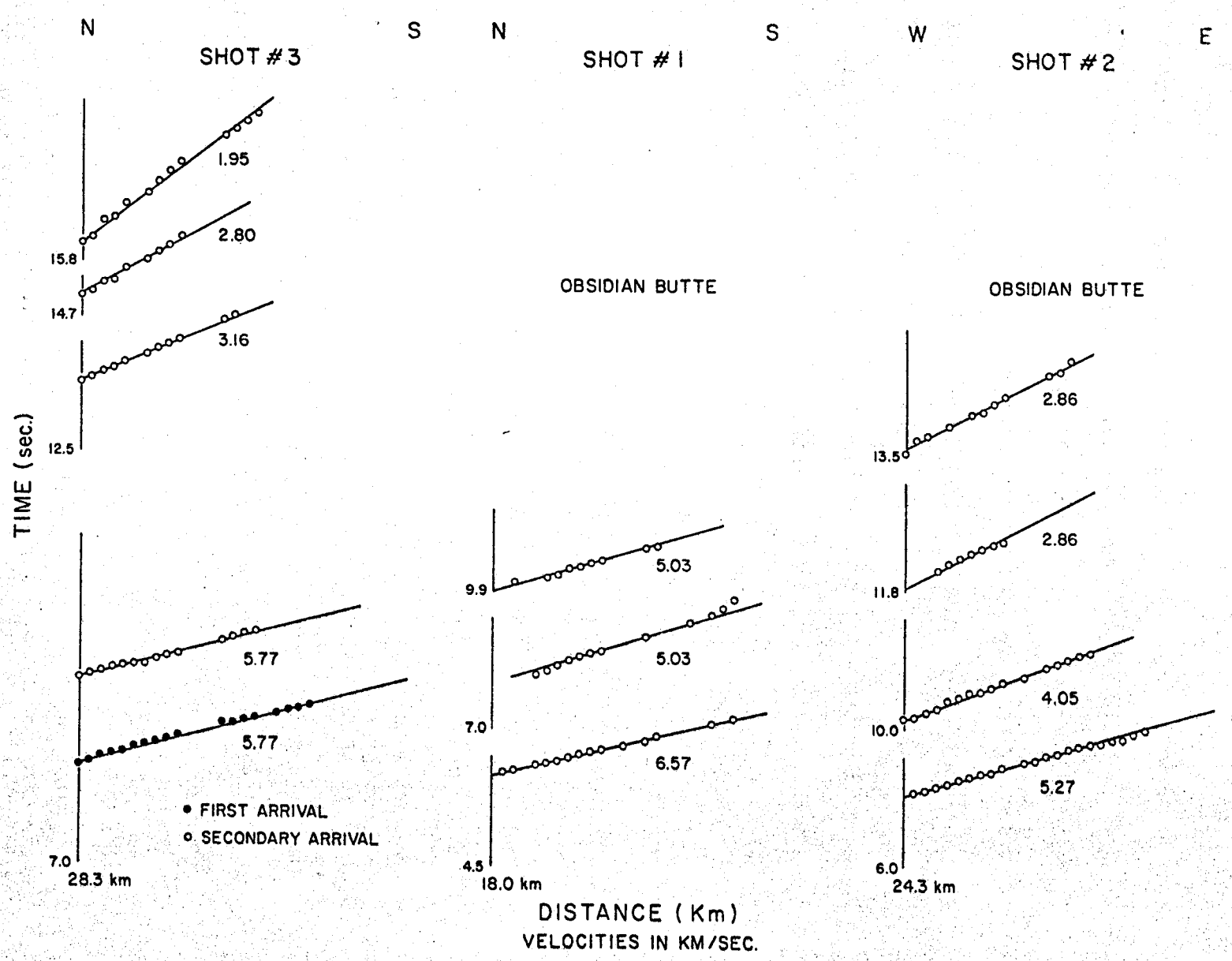

Figure 16

Plot of arrivals obtained from long-distance refraction shots 1, 2, 3.

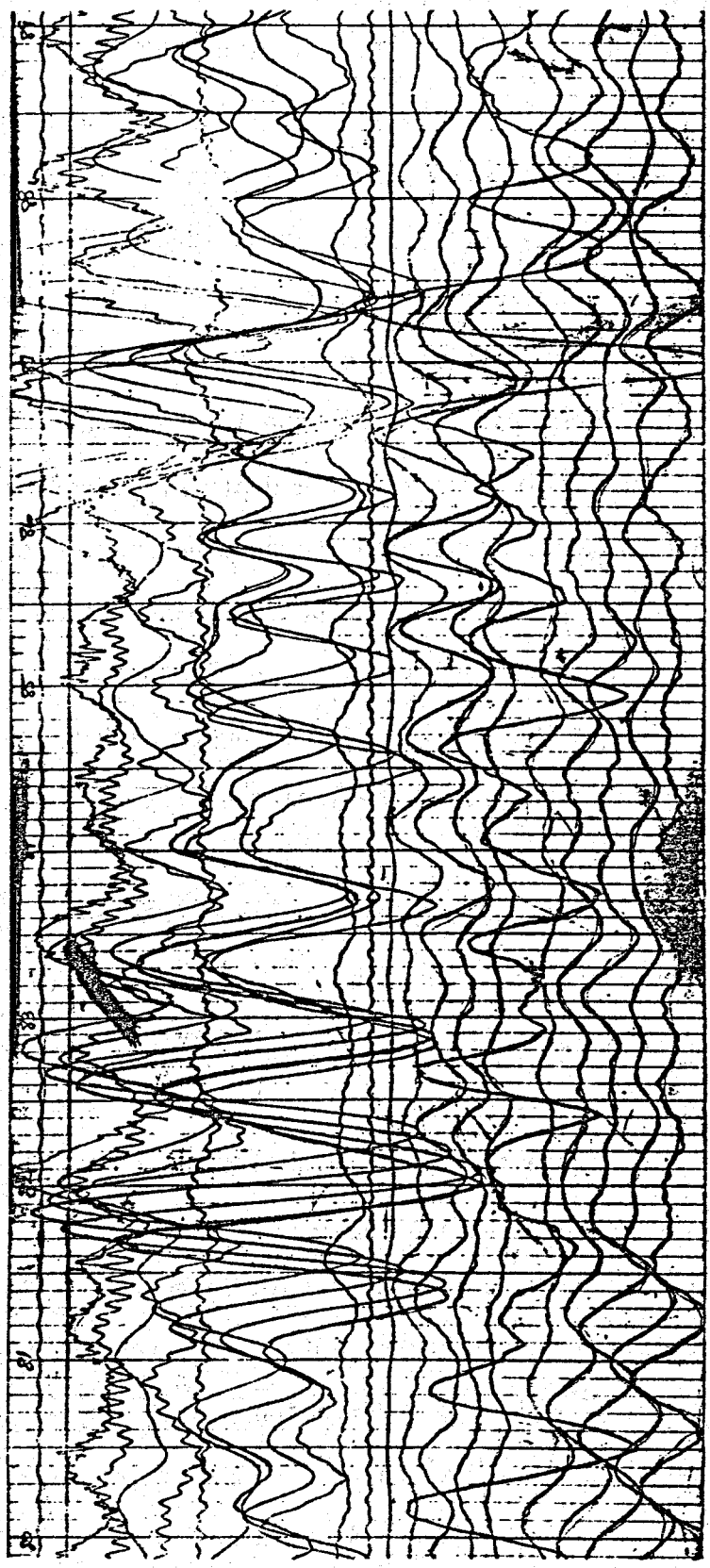

Figure 17

Portion of shot 3, recording 8.0 to 8.9 sec. Timing lines are spaced at 0.01 sec intervals. Emergent high amplitude events begin at approximately 8.2 and 8.6 sec.

Following the first arrivals, emergent high amplitude events were observed beginning at 8.2 sec (Figure 17.). The high amplitude of these events is suggestive of reflections (personal communication, Biehler, 1978). Assuming these events are reflections, and given the shot point to detector distance of 29 km and a constant average sedimentary section velocity of 3.9 km/sec (consistent with velocity information from Profiles 1-5), the two-way travel time of 8.2 sec implies a reflecting horizon at a depth of approximately 6.6 km. This depth is consistent with proposed basement depths in the Imperial Valley. Biehler (1964) has proposed a basement depth of 6 km, and analysis of Profile 2 yields a depth of 6.6 km. The close agreement of the computed two-way travel time depth with proposed basement depths suggests the events beginning at 8.2 sec are indeed reflections from basement.

Beginning at approximately 8.6 sec (Figure 17), a second set of emergent high amplitude arrivals were observed. The arrivals at geophones most distant from the shot point come in sooner than arrivals at the closer geophones. Assuming these arrivals are reflections (suggested by the high amplitudes), reflecting horizon depths can be computed that fit the two-way travel time of approximately 8.6 sec. Unpublished seismic velocity data based on numerous seismic station recordings of Shot 3 (courtesy of Hadley, 1978), provide crustal velocity information. Best fit of the crustal data expressed by the first seven data points shown in Figure 18 yields a range of 5.7 to 6.3 km/sec. Assuming a horizontal reflecting surface and a constant average crustal velocity of 5.7 km/sec (consistent

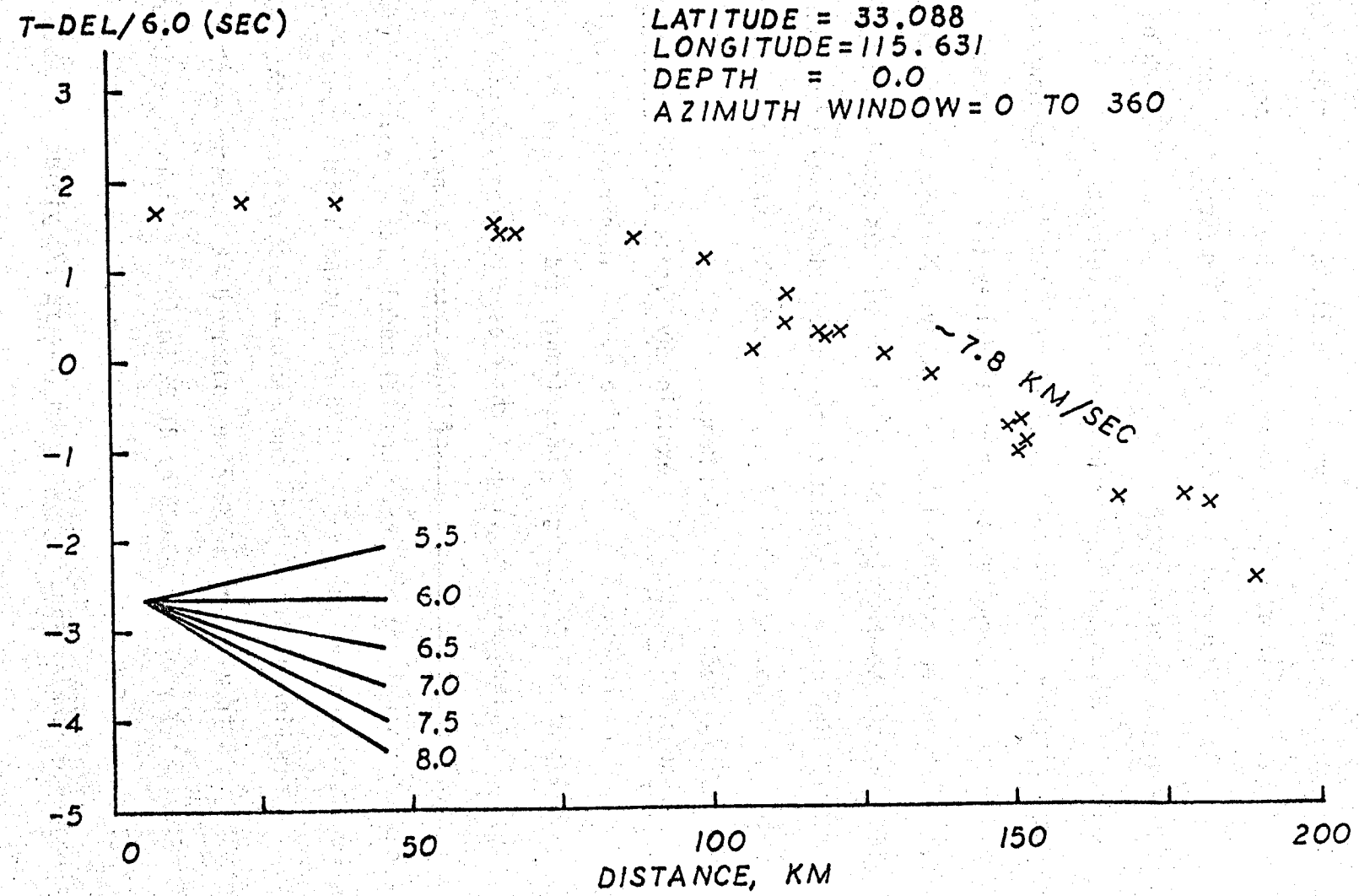

Figure 18

Reduced-time plot of Shot 3, based on permanent U.S.G.S. and portable station recordings (unpublished data, courtesy of D. M. Hadley, 1978).

with velocity information from Profile 2), a depth on the order of 20 km is consistent with a two-way travel time of 8.6 sec. Assuming a constant average crustal velocity of 6.3 km/sec, a depth of 23 km is consistent with an 8.6 sec two-way travel time, and a depth of 22 km is consistent assuming an average crustal velocity of 6.0 km/sec. These computed depths are consistent with the depth to Mohorovicic discontinuity (Moho) in the Imperial Valley (21 km) proposed by Biehler (1964) based on a regional gravity study. A minimum depth to Moho of 18 km at the head of the Gulf of California was determined by Phillips (1964). The close agreement of the computed two-way travel time depths with the proposed depth to Moho, suggests the arrivals beginning at 8.6 sec are reflections from Moho.

The problem remains to explain why events arrive sooner at the farther geophones. The travel time of the inferred Moho reflections arriving at the farther geophones (south end of spread) is less than that of reflections arriving at the closer geophones (north end of spread). This suggests a dip of Moho toward the north could be the cause. Assuming a one-layer crustal model with a constant average crustal velocity, the depth to the reflecting horizon can be solved as a function of travel time and measured distance from the shot point. A travel time of 8.62 sec observed at a distance of 29.50 km (Figure 17) yielded a depth of 21.22 km (assuming an average crustal velocity of 6.0 km/sec). Similarly, a travel time of 8.63 sec observed at a distance of 29.30 km (Figure 17) yielded a depth of 21.35 km. The difference in depth of 0.13 km within the horizontal distance of 0.20 km yields a dip on the order of 30 degrees.

Admittedly, the calculation is very crude and subject to error because of the limited data base. However, the calculation does show that a sharp local dip of Moho could explain reflections arriving earlier at the farther geophones. A regional dip of Moho of approximately 10 degrees toward the north has been proposed by Hadley (1978) based on P-delay studies in the Imperial Valley. Additional information is needed to resolve the problem of the early arrivals at the farther geophones.

Shot 4

The arrivals of this shot are included in the seismic data of Profile 1 (Figure 5).

First arrivals were weak and could not be read accurately. Weak secondary arrivals of 5.49 km/sec were observed. Based on their low-frequency signature, the 5.49 km/sec arrivals are interpreted as basement events. Later occurring arrivals were weak and could not be read accurately.

REFRACTION PROFILE INTERPRETATIONS

The seismic profile interpretations were constructed using information obtained from time-intercept formulas developed by Mota (1954) for reversed seismic refraction profiles. In preparing the seismic models, data from all profiles were used to infer the existence of seismic layers not detected in either forward or reverse direction recordings. Use of controls on depth calculations, obtained from sites where the seismic profiles intersect and calculated depths of the seismic velocity layers interpreted as identical should agree, have also been incorporated into the construction of the profile interpretations. Discrepancies in calculated depths at these depth-control intersection sites have been used to infer structures that would affect the calculated layer thickness.

Data from wells within the geothermal area was not useful in the preparation of the seismic interpretation models. The well locations were not adjacent to the seismic profile lines, and did not reach sufficient depths to aid in the resolution of deep seismic layers (greater than 3 km) or basement. The deepest wells reached depths of 2100-2400 meters, but core data was limited. Information from shallower wells is of little use in the matter of seismic layers at depth.

All profiles were interpreted assuming the presence of the 0.35 km/sec seismic layer detected in Profile 1. In support of this assumption are the close proximity of the profiles to each other and strong similarities in the near-surface sedimentary cover observed in shot holes. The calculated thickness of the 0.35 km/sec layer varied

TABLE 3

SUMMARY OF SEISMIC VELOCITIES, DIP ANGLES, AND LAYER THICKNESSES FOR PROFILES 1-6

Profile	Apparent Velocity (km/sec)		True Velocity (km/sec)	Dip Accuracy ±10%	Layer Thickness (km)		Altered Thickness (km)****	
	Forward	Reverse			Forward	Reverse	Forward	Reverse
1	1.70	1.70	1.70	0	0.12	0.15	----	----
	1.98	1.98	1.98	0	0.44	0.69	----	----
	2.86	2.80	2.83	0.5°W	0.27	0.36	----	----
	4.05	4.05	4.05	0.5°E				
	4.63	5.03	4.82	4.0°E	?	2.41	1.07	----
	5.49***	7.07	6.13	7.5°E	?	1.40	3.08	----
1*	1.70	1.70	1.70	0	0.12	0.15	----	----
	1.98	1.98†	1.98	0	0.59	0.59	----	----
	4.05	4.05†	4.05	0	1.07	1.07	----	----
	----	4.51	4.51	0				
2	1.70	1.70†	1.70	0	0.09	0.06	----	----
	1.95	1.95	1.95	0	0.32	0.78	----	----
	2.80	2.80	2.80	0	0.76	1.11	----	----
	3.66	3.72	3.69	0.5°S	1.95	1.10	0.66	----
	5.18	5.18†	5.18	0.5°N	2.13	3.61	3.44	----
	5.97**	6.40	6.16	2.75°S				
3	1.70†	1.70	1.70	0	0.18	0.18	0.09	----
	1.98†	1.98	1.98	0	0.36	0.64	0.46	----
	2.86	2.80†	2.83	0.5°W	1.06	0.84	0.62	0.58
	4.05†	4.05†	4.05	0.5°E	0.09	0.52	0.53	1.22
	4.63†	5.03	4.82	3.75°E				
4	1.70†	1.70	1.70	0	0.18	0.18	0.09	----
	1.98†	1.98	1.98	0	0.41	0.64	0.50	----
	2.86	2.80†	2.83	0.5°W	1.08	0.93	0.96	----
	4.05†	4.05†	4.05	0.5°E	0.32	0.85	0.44	----
	4.63†	5.03	4.82	3.75°E				
5	1.70	1.70	1.70	0	0.18	0.18	----	----
	1.95	1.95	1.95	0	0.63	0.54	----	----
	2.80	2.80	2.80	0	0.56	0.73	0.27	1.05
	3.66	3.72†	3.69	0.5°S	1.10	1.02	1.40	0.72
	5.18†	5.18	5.18	0				
6	1.95	----	1.95	0	0.76	----	----	----
	2.80	----	2.80	0	0.69	----	----	----
	3.72	----	3.72	0				

†Layer existence inferred from other profiles
**Obtained from Shot 3
***Obtained from Shot 4
****Inferred from depth-control points

from 1.8 to 5.3 meters, and was excluded from presentation in the seismic profile models.

A summary of the information contained in the profile interpretations is contained in Table 3.

Profile 1

Two interpretations of Profile 1, differing only in basement dip in the east-west direction, are presented in Figures 19 and 20. Both interpretations show a fault occurring within the sedimentary section between 3 and 4 km from Obsidian Butte. The throw and location of faulting in the 1.98 and 2.83 km/sec seismic layers are poorly constrained, as this interpretation was based on secondary arrivals. The throw (215 meters) and location of faulting in the 4.05 km/sec seismic layer were computed from the 0.1 sec time delay observed in the first arrivals. Arrivals from the 4.82 and 6.13 km/sec seismic layers gave no apparent indication of faulting.

The seismic layers of the sedimentary section, with one exception, have very shallow dips (less than 1 degree). The exception, the 4.82 km/sec seismic layer, has an easterly dip calculated to be 4 degrees ($\pm$ 10%).

The point of intersection with Profile 5 is indicated in Figures 19 and 20. The agreement in calculated depths, with one exception (refer to Profile 5 interpretation), was very good, with no differences greater than 10%.

The high apparent basement velocity of 7.07 km/sec, recorded in the reverse direction of Profile 1, can be explained with the basement

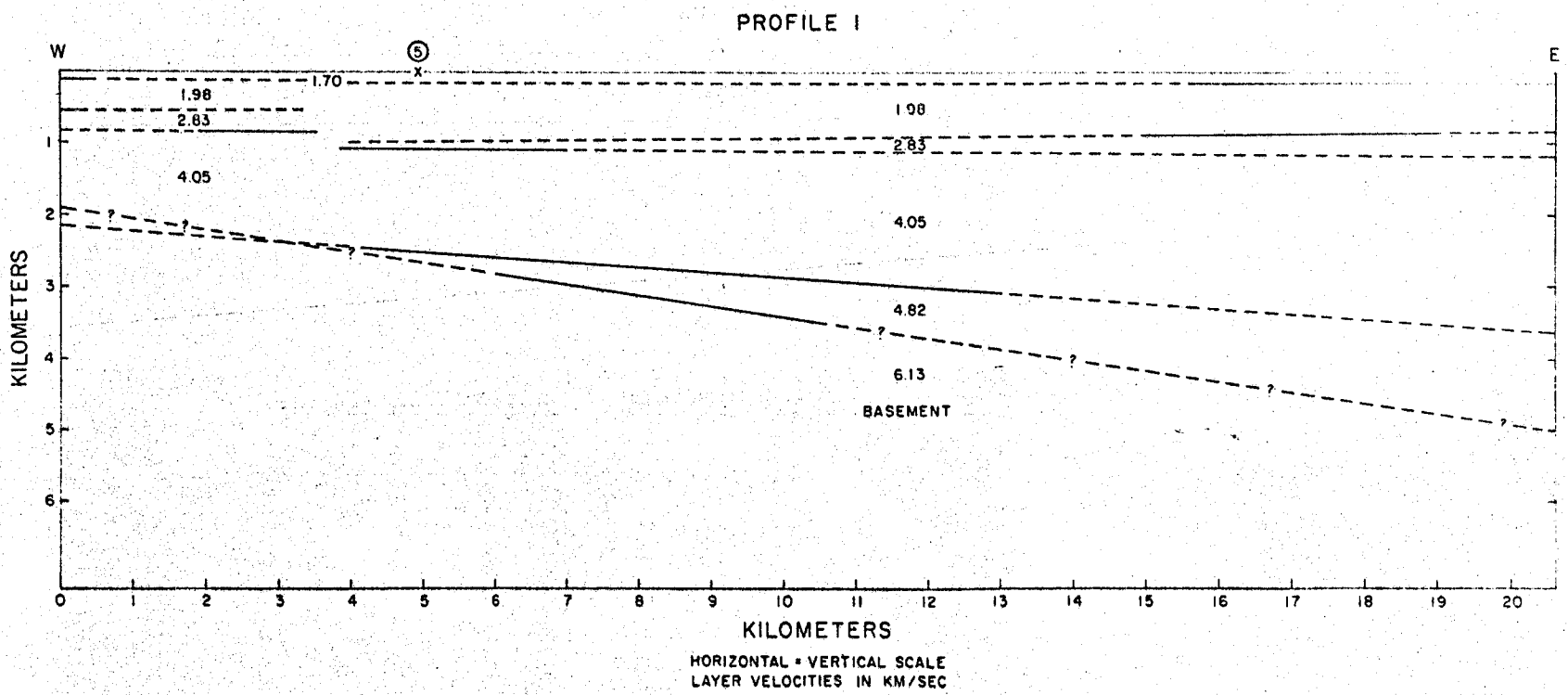

Figure 19

Seismic interpretation of Profile 1 with proposed eastward dip of basement. The intersection point with Profile 5 is indicated. Solid lines represent sections of seismic layers interrogated by the profile; dashed lines represent extrapolations. Dashed lines with question marks represent basement extrapolations.

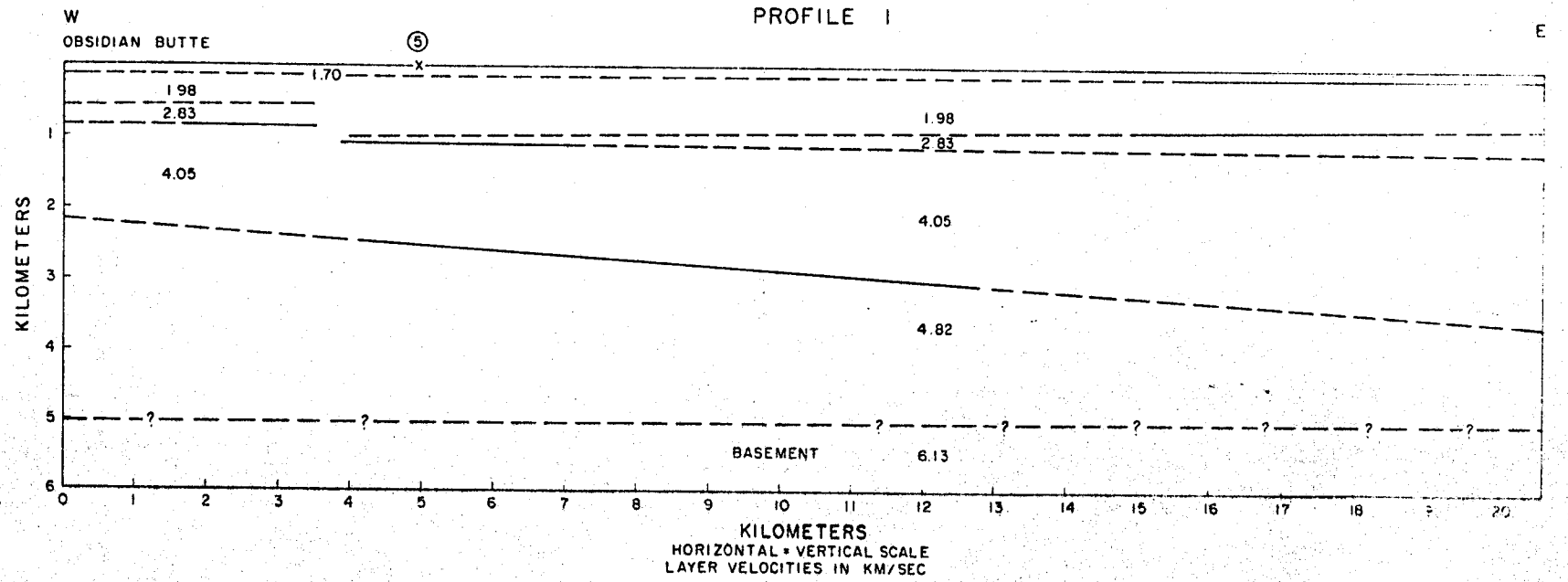

Figure 20

Seismic interpretation of Profile 1 with assumed horizontal basement. A seismic velocity gradient is proposed that increased the apparent basement velocity from east to west by approximately 15%. Solid lines represent sections of seismic layers interrogated by the profile; dashed lines represent extrapolations. The dashed line with question marks represents the assumed horizontal basement interface.

models shown in Figures 19 and 20. The interpretation presented in Figure 19 shows basement dipping sharply to the east with a calculated dip of 7.5 degrees. The dip to the east produces an increasing basement depth that is consistent with the absence of basement arrivals from recordings of the forward direction (shooting toward the east), and yields the high apparent up-dip velocity (7.07 km/sec) in the reverse direction. Extrapolating basement to the west (denoted by question marks) yields a depth of 2 km at Obsidian Butte, and to the east a depth of 5 km at East Highline Canal. Sufficient data are not available to resolve the 4.82 km/sec and basement interfaces at the west end of the profile. The interpretation presented in Figure 20 shows a horizontal basement interface. A seismic velocity gradient is proposed that increases the apparent velocity from east to west by approximately 15% in the basement within the geothermal area. The amount of increase was calculated assuming a linear velocity increase, based on an initial velocity of 6.2 km/sec (consistent with velocity information from Profile 2 and long distance shots 1 and 3). The assumed horizontal basement, at the depth of 5 km calculated at the east end of the profile (based on data contained in Table 3), together with the proposed seismic velocity gradient from east to west yield the high apparent basement velocity of 7.07 km/sec observed in the reverse profile.

The arrivals occurring between 1 and 1.5 km in the forward profile (Figure 5) that depart from a fit to 1.70 km/sec are interpreted as first arrivals from the 2.83 km/sec seismic layer. This interpretation is based on the 2.86 km/sec apparent velocity obtained through a best fit of the arrivals and travel time calculations.

Calculated travel times indicate that thinning of the 1.98 km/sec seismic layer by approximately 0.25 km in the range between 1 and 1.5 km (assuming remaining layers are constant in thickness) would allow first arrivals from the 2.83 km/sec seismic layer to occur between 1 and 1.5 km. Outside this range, arrivals from the 1.98 and 2.83 km/sec seismic layers occur as secondary events. Local thinning of the 1.98 km/sec seismic layer is therefore proposed to explain the occurrence of first arrivals from the 2.83 km/sec seismic layer between 1 and 1.5 km. The proposed thinning is not shown in Figures 19 and 20 so as to avoid confusion with offsets inferred from more accurate depth-control information.

Profile 1*

The seismic interpretation of Profile 1* is presented in Figure 21. The 1.98, 4.05 and 4.51 km/sec seismic layers are interpreted as horizontal, due to a lack of reversal information.

Arrivals of 4.51 km/sec were not observed in any other profile of this investigation. It is unlikely therefore that these arrivals result from a previously undetected seismic layer. In view of historic volcanism in the area, it is possible these arrivals are refractions from dike-swarms or flows that have intruded the sedimentary section.

As Profile 1* (forward direction) was identical with the forward direction line of Profile 1, and both profiles had common shot point and geophone spread locations, the arrivals showing departure from a fit to 1.70 km/sec beginning at 1 km in both profiles must result from the same source. Lack of recordings in Profile 1* prevented the

observance of arrivals from the 2.83 km/sec seismic layer. For further discussion, refer to the interpretation of Profile 1.

Profile 2

The seismic interpretation of Profile 2 is presented in Figure 22. Discrepancies in calculated seismic layer depths at the points where Profiles 3, 4 and 6 intersect Profile 2 have been used to infer faults in the sedimentary section between the zero-point and 6 km. The throws and locations of faulting cannot be precisely detailed with the existing data, as the depth-control information from Profiles 3 and 4 rely on extrapolations of seismic layer interfaces.

With one exception, the interpreted seismic layers have very shallow dips. Calculated dips of the sedimentary seismic layers were less than one degree (± 10%). The exception, basement, has a calculated dip of 3 degrees to the south. Extrapolating basement to the north yields a depth of 5.2 km at Obsidian Butte. An extrapolation of basement to the south yields a depth of 6.6 km near Brawley, California (Figure 1).

At the site where the Westmoreland profile (Biehler, 1964) intersects Profile 2, calculated depths of seismic layers are in excellent agreement.

The absences of certain seismic layer arrivals from recordings of the forward or reverse direction are consistent with the seismic interpretation of Profile 2. The absence of 1.70 km/sec arrivals from the reverse direction recordings is consistent with the thinning of the 1.70 km/sec seismic layer to the south. The absence of 5.18 km/sec arrivals from reverse direction recordings may be due to weak

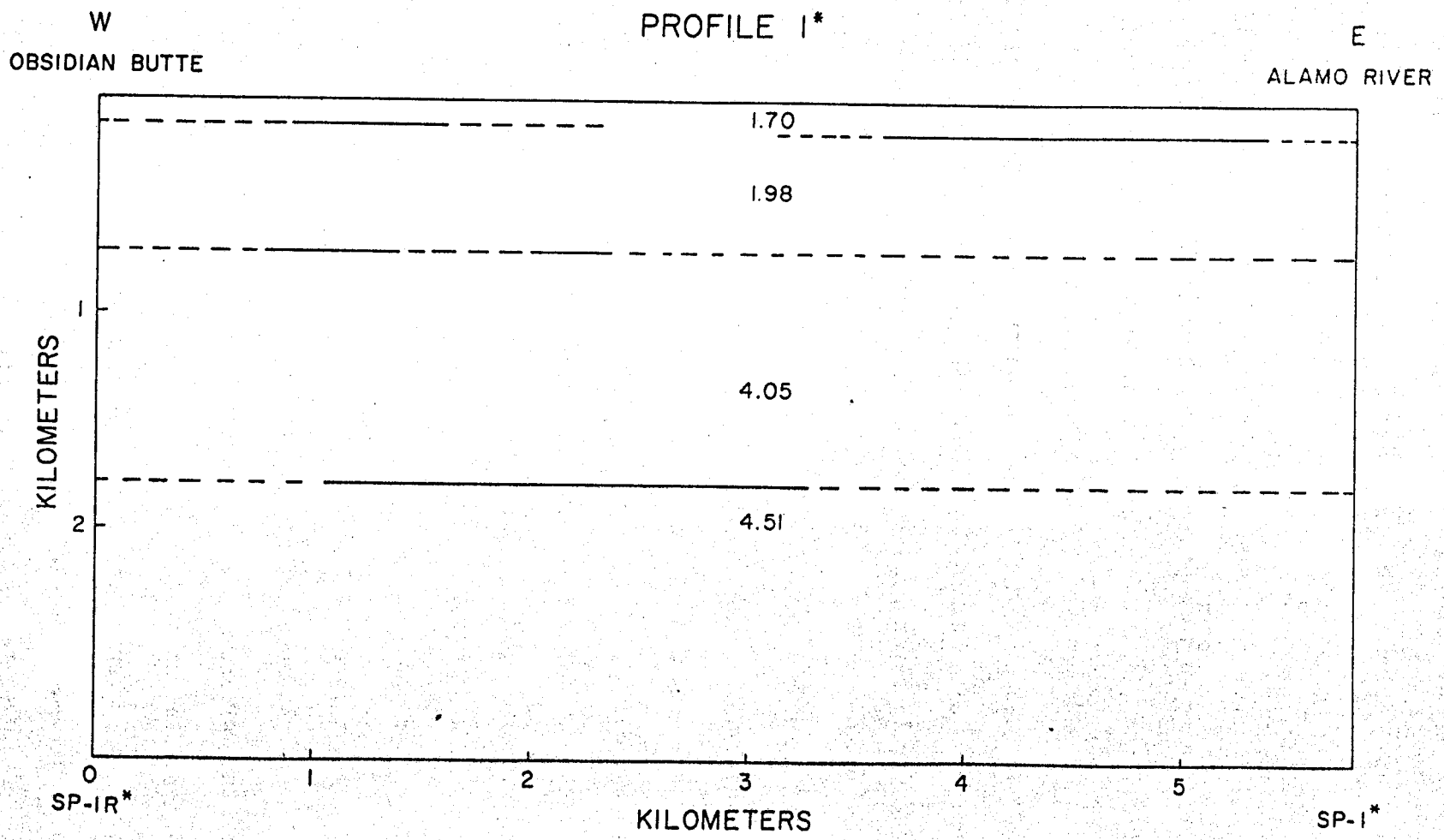

Figure 21

Seismic interpretation of Profile 1*. Solid lines represent sections of seismic layers interrogated by th[illegible] dashed lines represent

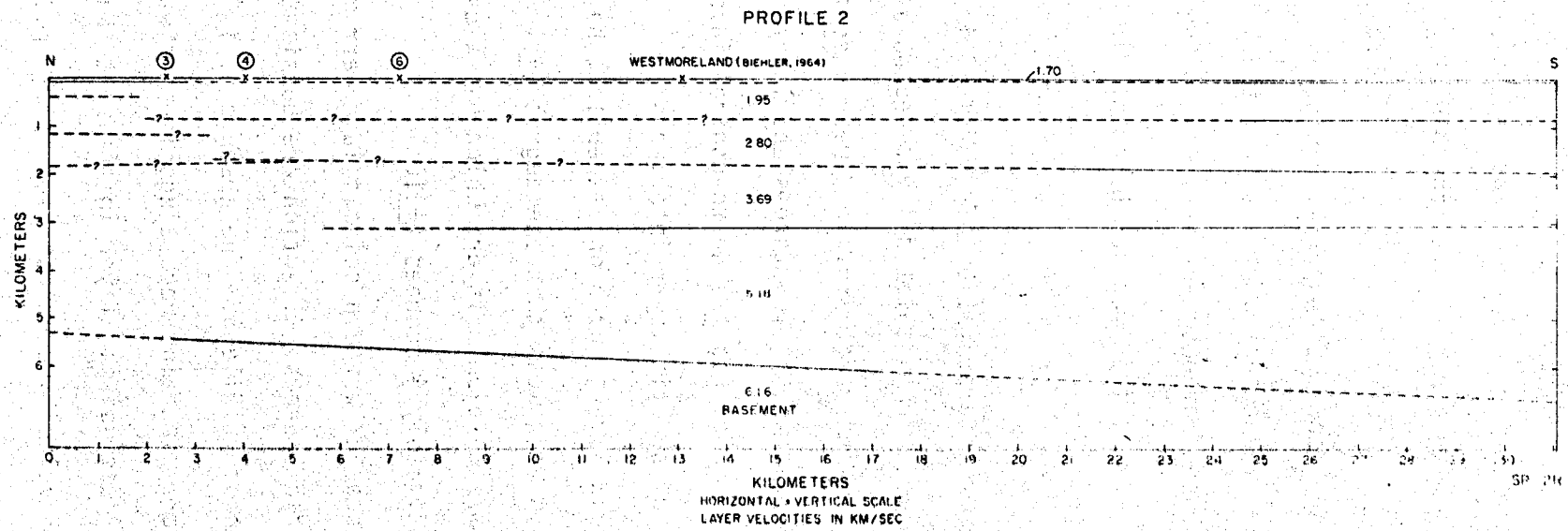

Figure 22

Seismic interpretation of Profile 2. Intersection points with Profiles 3, 4, and 6 are indicated. Solid lines represent sections of seismic layers interrogated by the profile; dashed lines represent extrapolations. Dashed lines with question marks represent extrapolations based on depth-control information.

first energy or masking. The decrease in basement depth to the north, creating a velocity contrast with the 3.69 km/sec seismic layer of approximately 1.75 to 1, together with the gradual thinning of the 5.18 km/sec layer toward the north, could have been capable of concealing the presence of arrivals from the 5.18 km/sec seismic layer. The absence of basement arrivals in the forward direction could be a result of the proposed basement dip to the south.

Profile 3

The seismic interpretation of Profile 3 is presented in Figure 23. Discrepancies in calculated layer depths at the points where Profiles 2 and 5 intersect Profile 3 were used to infer faults in the sedimentary section. The throws and locations of faulting cannot be precisely detailed, as the depth-control information relies on the extrapolation of seismic layer interfaces.

The seismic layers, with one exception, have very shallow dips. Calculated dips were less than one degree ($\pm$ 10%), with the exception of the 4.82 km/sec seismic layer, which has a calculated dip to the east of approximately 4 degrees ($\pm$ 10%).

The absences of certain seismic layer arrivals from recordings of the forward or reverse direction are consistent with the seismic interpretation of Profile 3. The absence of 1.98 km/sec arrivals from the forward direction recordings is consistent with the thinning of the 1.98 km/sec seismic layer in the west (based on travel times) and the larger velocity contrast (1.7 to 1) produced by the shallow 2.83 km/sec seismic layer with the 1.70 km/sec seismic layer. The

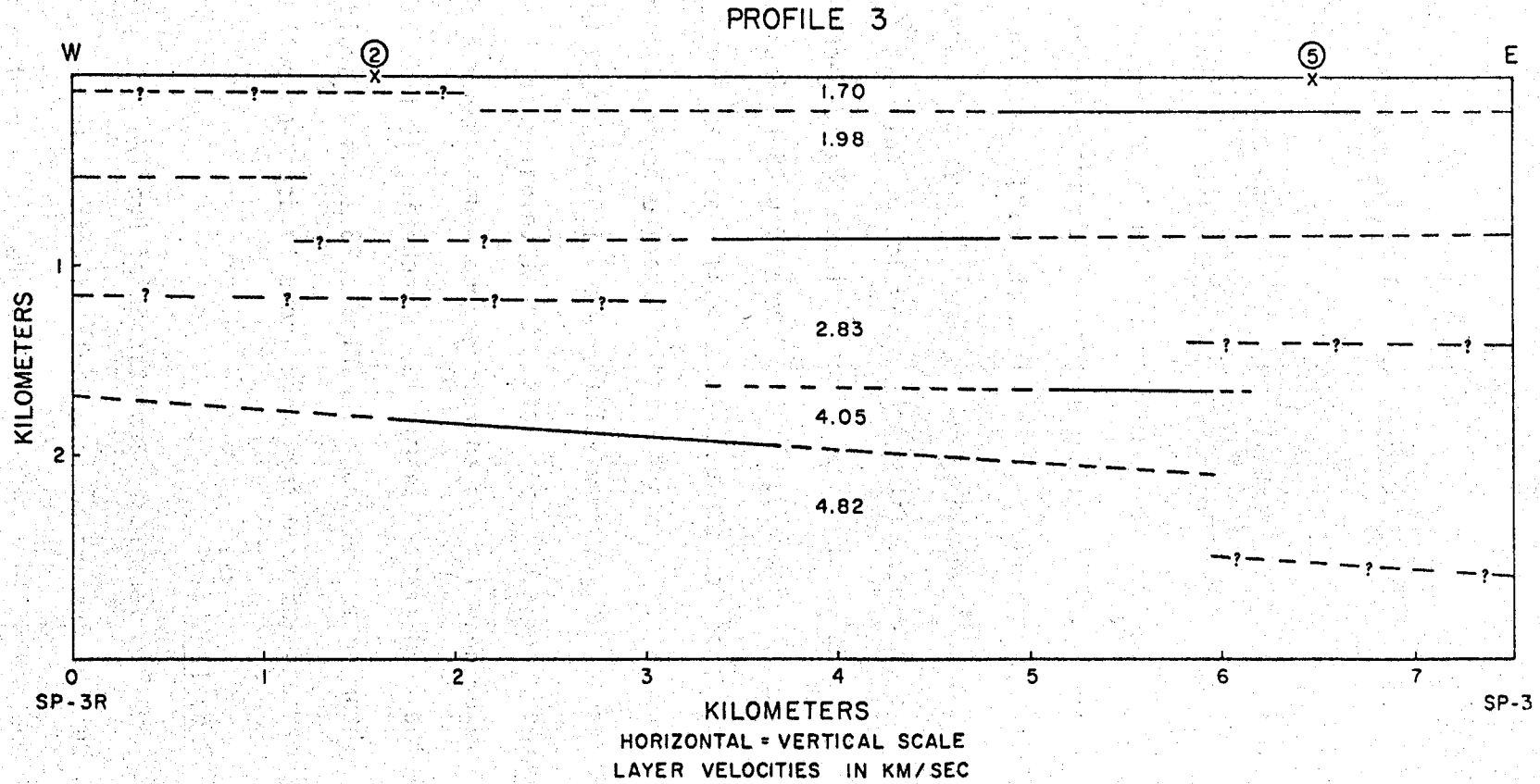

Figure 23

Seismic interpretation of Profile 3. Intersection points with Profiles 2 and 5 are indicated. Solid lines represent sections of seismic layers interrogated by the profile; dashed lines represent extrapolations. Dashed lines with question marks represent extrapolations based on depth-control information.

absence of 4.82 km/sec seismic layer arrivals from the forward direction recordings is consistent with the increasing depth to the 4.82 km/sec layer produced by the eastward dip. The absence of 4.05 km/sec arrivals from recordings of the reverse direction is consistent with the proposed thinning of the 4.05 km/sec seismic layer.

The arrivals beginning at 1 km in the forward profile direction (Figure 12) that show an apparent depart from linearity are interpreted as first arrivals from the 2.83 km/sec seismic layer. This interpretation is based on the 2.86 km/sec apparent velocity obtained through a best fit of the arrivals and calculated travel times. Calculation of travel times indicate that a decrease in the thickness of the 1.98 km/sec seismic layer of 0.25 km (assuming the remaining layers are constant in thickness) near 1 km would allow first arrivals from the 2.83 km/sec seismic layer to begin at 1 km. At distances less than 1 km, arrivals from the 1.98 and 2.83 km/sec seismic layers occur as secondary events. Local thinning of the 1.98 km/sec seismic layer near 1 km is therefore proposed to explain first arrivals from the 2.83 km/sec seismic layer occurring at 1 km. The proposed thinning is not shown in Figure 23 so as to avoid confusion with offsets inferred from more accurate depth-control information.

Profile 4

The seismic interpretation of Profile 4 is presented in Figure 24. Discrepancies in calculated seismic layer depths at the point where Profile 2 intersects Profile 4 were used to infer faults in the sedimentary section. The throws and locations of faulting cannot be precisely detailed, as the depth-control information relies on the

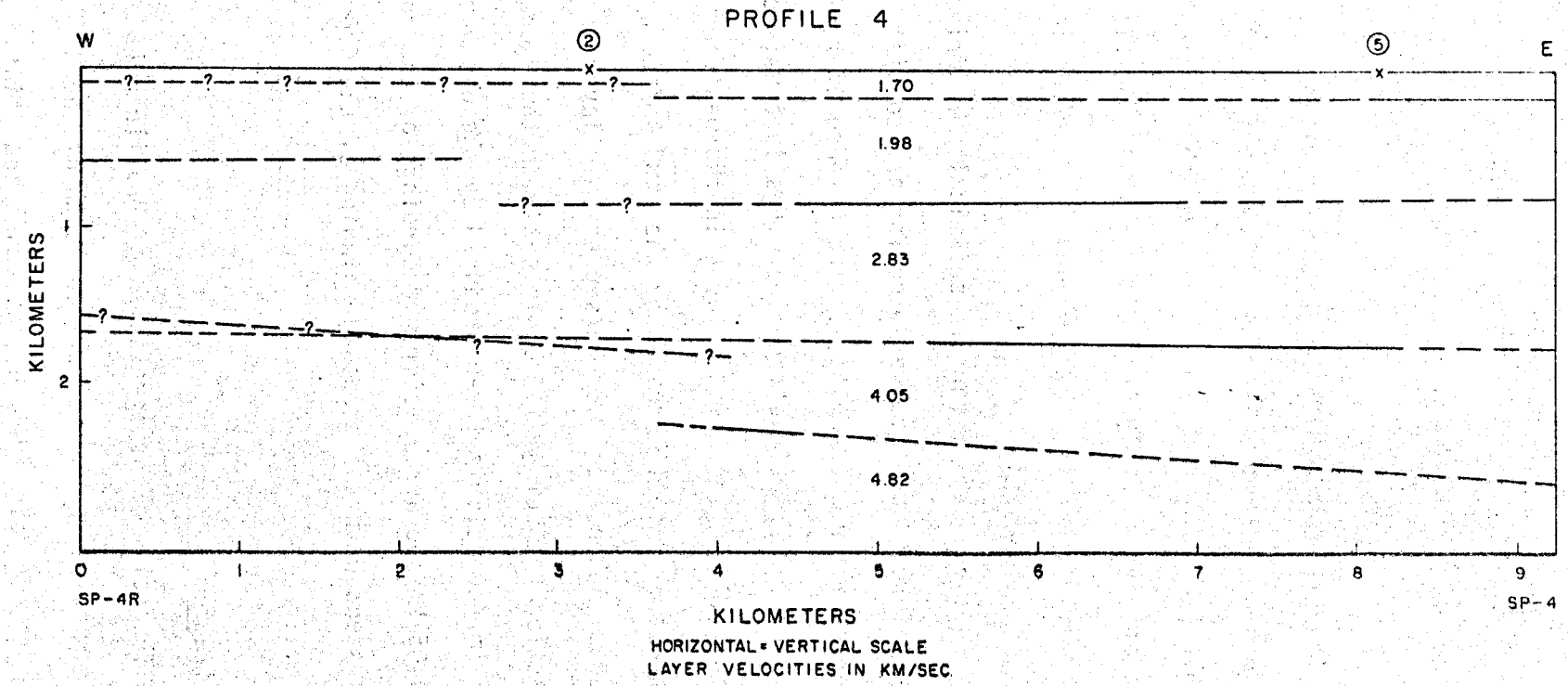

Figure 24

Seismic interpreation of Profile 4. Intersection points with Profiles 2 and 5 are indicated. Solid lines represent sections of seismic layers interrogated by the profile; dashed lines represent extrapolations. Dashed lines with question marks represent extrapolations based on depth-control information.

extrapolation of seismic layer interfaces. At the point of intersection with Profile 5, calculated seismic layer depths were in excellent agreement.

The seismic layers, with one exception, have very shallow dips. Calculated dips were less than 1 degree (± 10%), with the exception of the 4.82 km/sec seismic layer, which had a calculated dip to the east of approximately 4 degrees (± 10%). Sufficient data is not available to resolve the 4.05 and 4.82 km/sec interfaces at the west end of the profile.

The absences of certain seismic layer arrivals from recordings of the forward or reverse direction are consistent with the seismic interpretation of Profile 4. The absence of 1.98 km/sec arrivals from the forward direction recordings is consistent with the thinning of the 1.98 km/sec seismic layer in the west and the larger velocity contrast (1.7 to 1) creased by the 2.83 km/sec and 1.70 km/sec seismic layers. Absence of 4.82 km/sec seismic layer arrivals from the forward direction recordings is consistent with the increasing depth to the 4.82 km/sec seismic layer produced by the eastward dip. The absence of 4.05 km/sec arrivals from recordings of the reverse direction is consistent with the proposed thinning of the 4.05 km/sec seismic layer.

Profile 5

The seismic interpretation of Profile 5 is presented in Figure 25. Discrepancies in the calculated depth of the 3.69 km/sec seismic layer at the points where Profiles 1 and 4 intersect were used to infer faults in the sedimentary section. With one exception, the

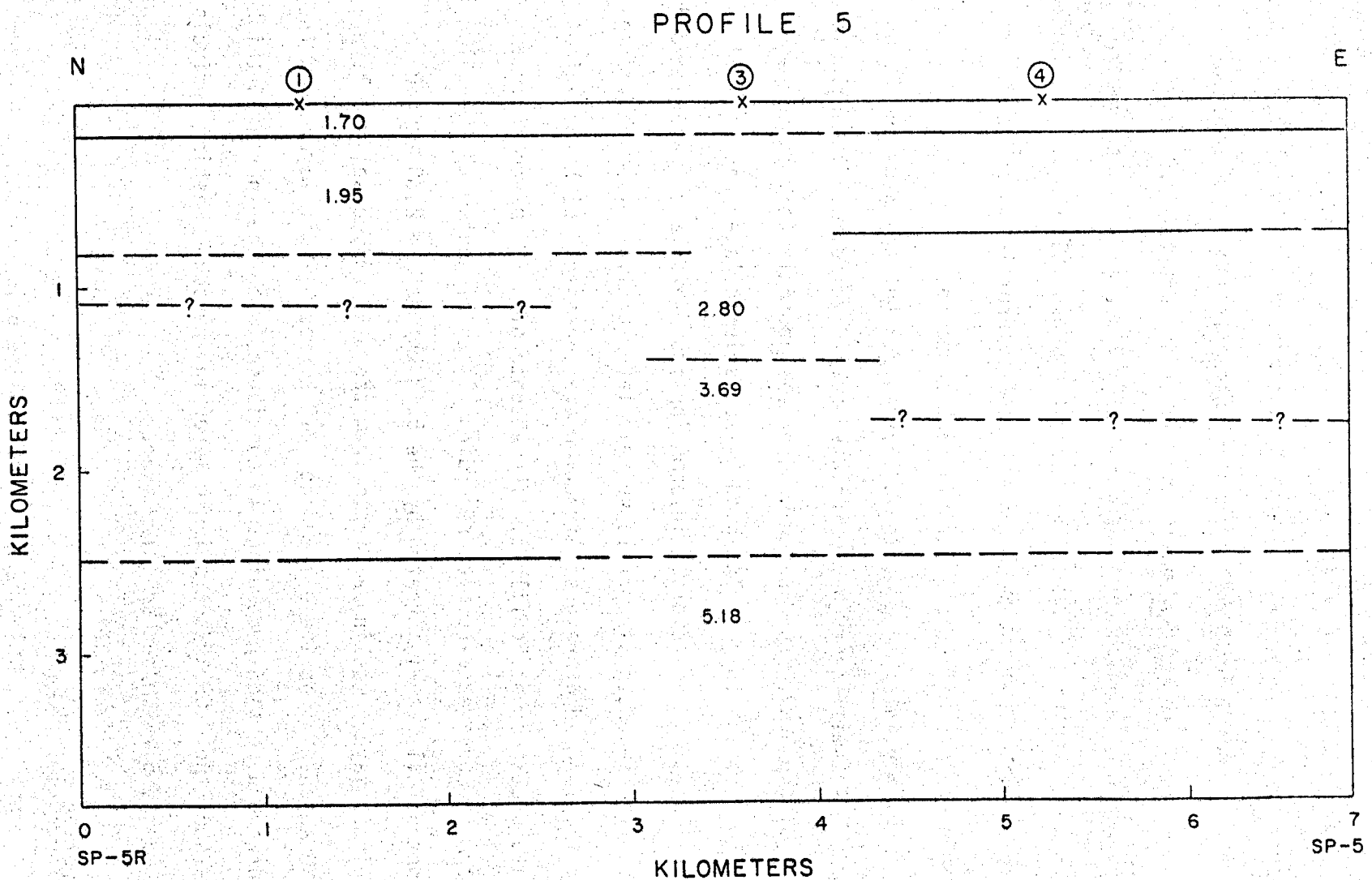

Figure 25

Seismic interpretation of Profile 5. Intersection points with Profiles 1, 3, and 4 are indicated. Solid lines represent sections of seismic layers interrogated by the profile; dashed lines represent extrapolations. Dashed lines with question marks represent extrapolations based on depth-control information.

throws and locations of faulting cannot be precisely detailed, as the depth-control information relies on extrapolation of seismic layer interfaces. The exception is the fault shown in the 2.80 km/sec seismic layer, which was based on the 0.07 sec offset observed in the first arrivals (Figure 15). The throw was calculated to be 100 meters. At the point of intersection with Profile 3, calculated depths of seismic layers were in good agreement.

Of the interpreted seismic layers, all but the 3.69 and 5.18 km/sec seismic layers had calculated horizontal dips. The calculated dip of the 3.69 km/sec seismic layer was approximately 1 degree ($\pm$ 10%) to the south. The 5.18 km/sec seismic layer was assumed horizontal, as no reversal information from this layer was recorded.

The absences of certain seismic layer arrivals from recordings of the forward or reverse direction are consistent with the seismic interpretation of Profile 5. The absence of 3.69 km/sec arrivals from the reverse direction recordings is consistent with the velocity contrast (1.9 to 1) created by the 5.18 km/sec and 2.80 km/sec seismic layers masking arrivals from the 3.69 km/sec seismic layer. The absence of arrivals from the 5.18 km/sec seismic layer from the forward direction recordings is consistent with the increased thickness of the 3.69 km/sec seismic layer in the south masking arrivals from the 5.18 km/sec seismic layer.

Profile 6

The seismic interpretation of Profile 6 is presented in Figure 26. The seismic layers shown are assumed horizontal, as this profile was

not reversed. At the points where Profiles 3 and 4 intersect, calculated seismic layer depths were in good agreement.

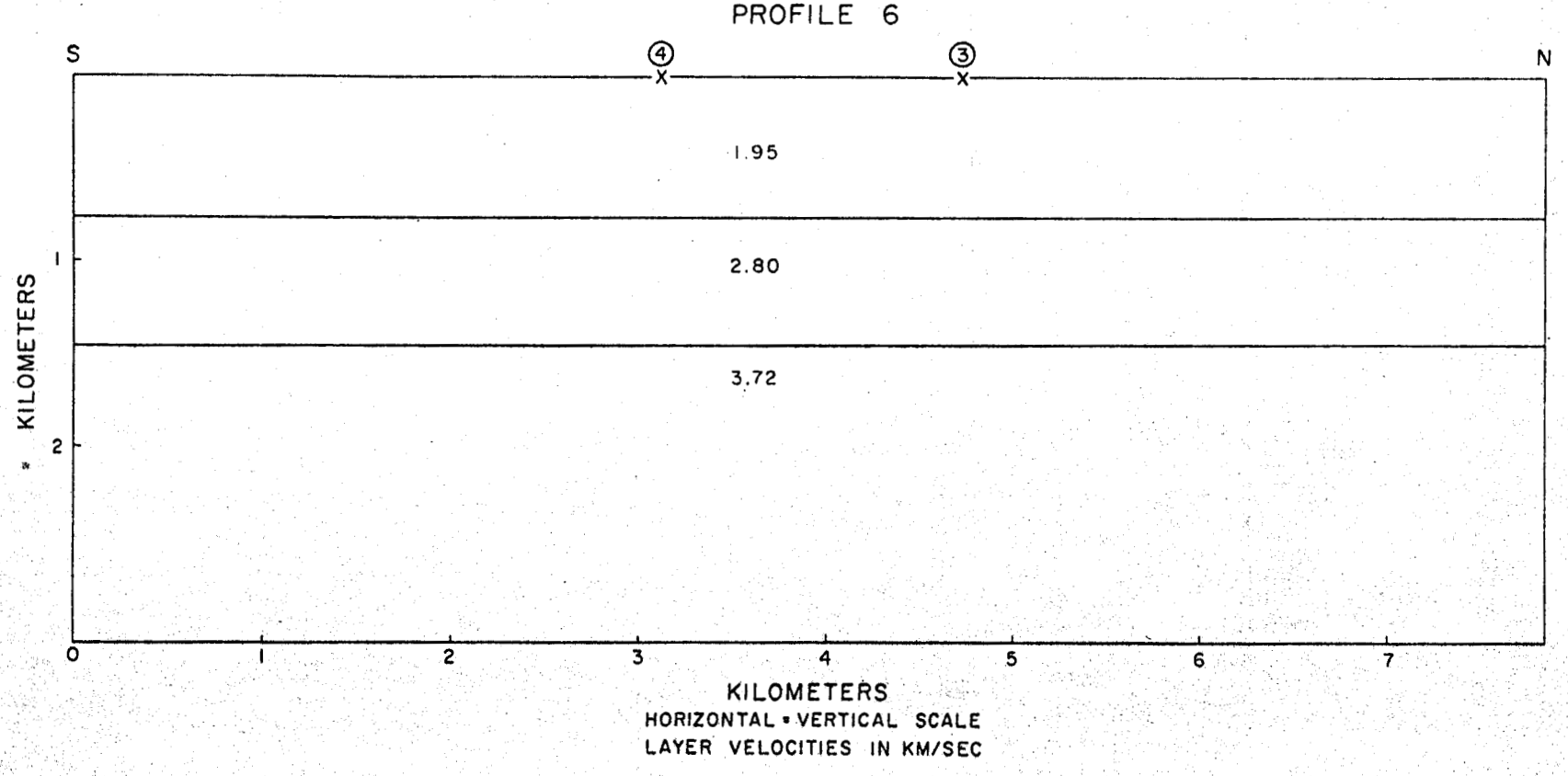

Figure 26

Seismic interpretation of Profile 6. Intersection points with Profiles 3 and 4 are indicated.

VELOCITY MODELS

From the seismic data and controls on calculated depths obtained from intersecting profiles, two three-dimensional models of the geothermal and adjacent area are proposed. "Model 1" is presented in Figure 27, and "Model 2" in Figure 28. The models show the sedimentary section is composed of nearly horizontal seismically defined layers. Calculated dips of the sedimentary seismic layers are less than 1 degree (± 10%), with the exception of the 4.82 km/sec seismic layer which has a calculated eastward dip of 4 degrees (± 10%). Agreement of seismic velocities of the sedimentary section is good, with no inconsistencies greater than 10%.

Based on the offsets inferred in the sedimentary section seismic layers shown in both models, two NW-SE trending fault zones are proposed. The respective locations are 3 km east and 2 km south of Obsidian Butte. Based on extrapolations, the existence of a third fault zone at Obsidian Butte may be indicated by the lack of agreement in the depth of intersecting seismic layers. The two proposed fault zones are consistent with microearthquake activity reported in the geothermal area. Gilpin (1977) and Johnson and Hadley (1976) show NW-SE trending lineations of epicenters adjacent Obsidian Butte. The locations of the two proposed fault zones are consistent also with the two fault locations surrounding Obsidian Butte (OBB) shown in Figure 29.

The basement interpretation proposed in Model 1 (Figure 27) is a high, trending parallel to the axis of the Imperial Valley. The high is implied by proposed dips of basement to the south

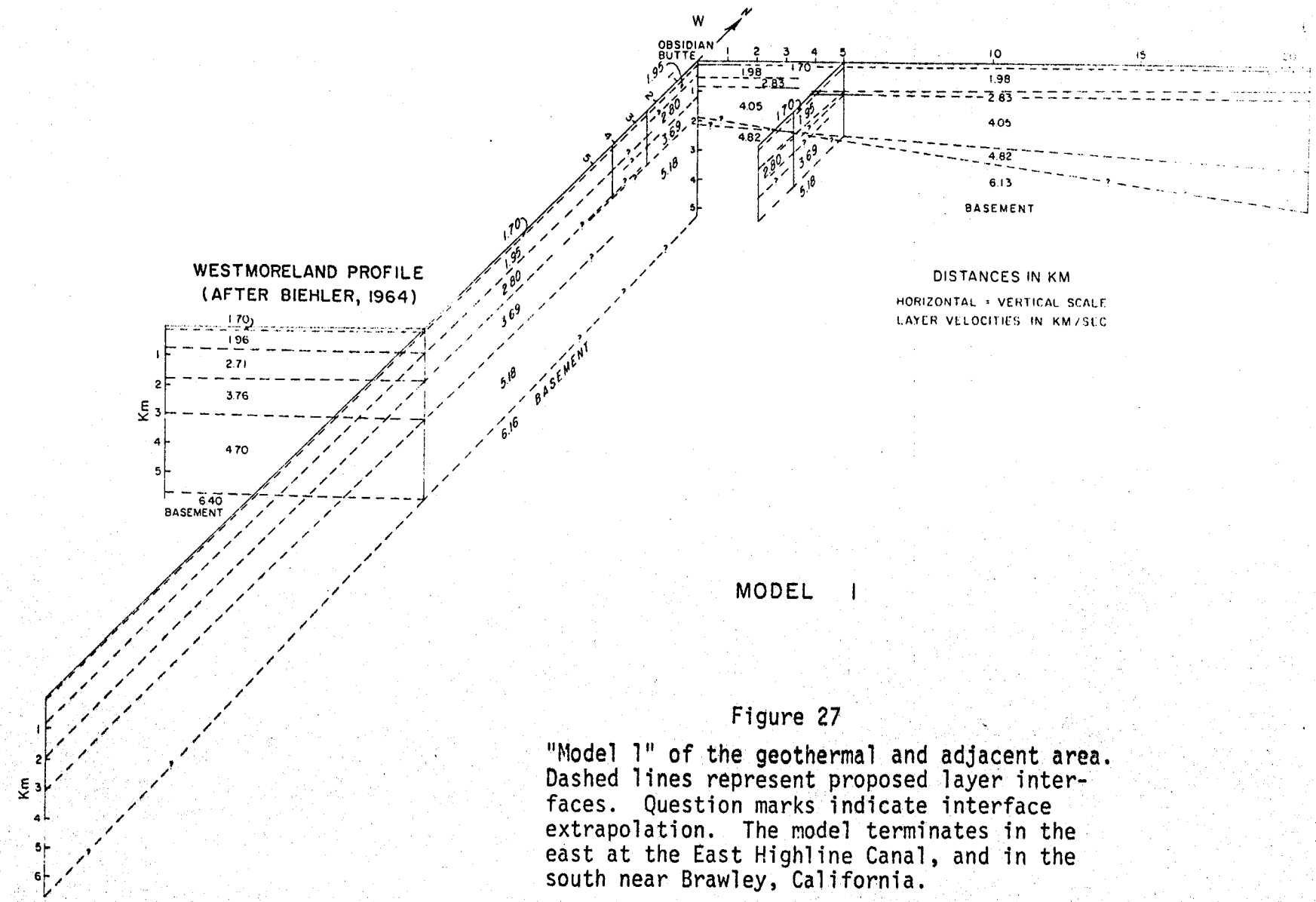

MODEL 1

Figure 27

"Model 1" of the geothermal and adjacent area. Dashed lines represent proposed layer interfaces. Question marks indicate interface extrapolation. The model terminates in the east at the East Highline Canal, and in the south near Brawley, California.

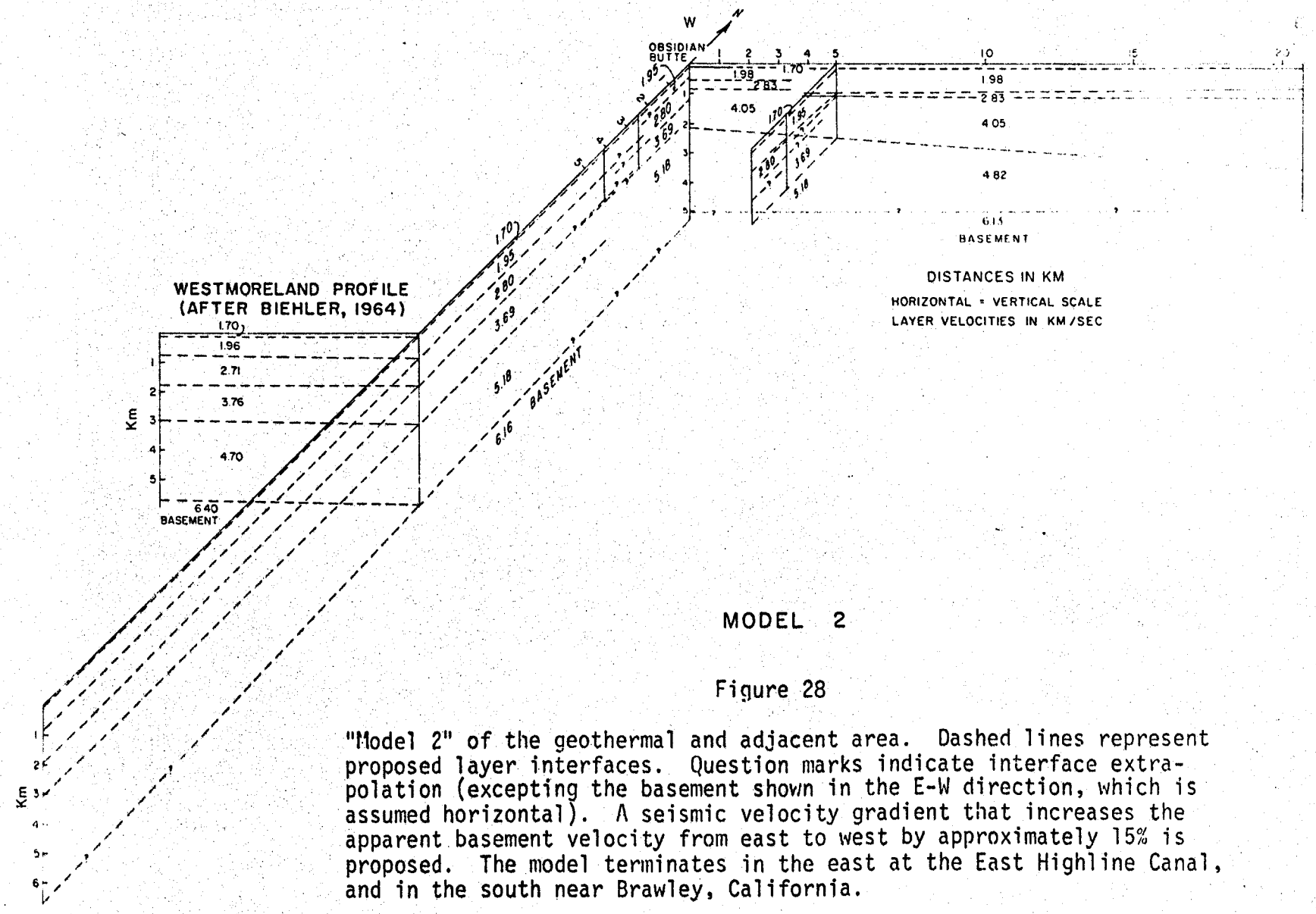

MODEL 2

Figure 28

"Model 2" of the geothermal and adjacent area. Dashed lines represent proposed layer interfaces. Question marks indicate interface extrapolation (excepting the basement shown in the E-W direction, which is assumed horizontal). A seismic velocity gradient that increases the apparent basement velocity from east to west by approximately 15% is proposed. The model terminates in the east at the East Highline Canal, and in the south near Brawley, California.

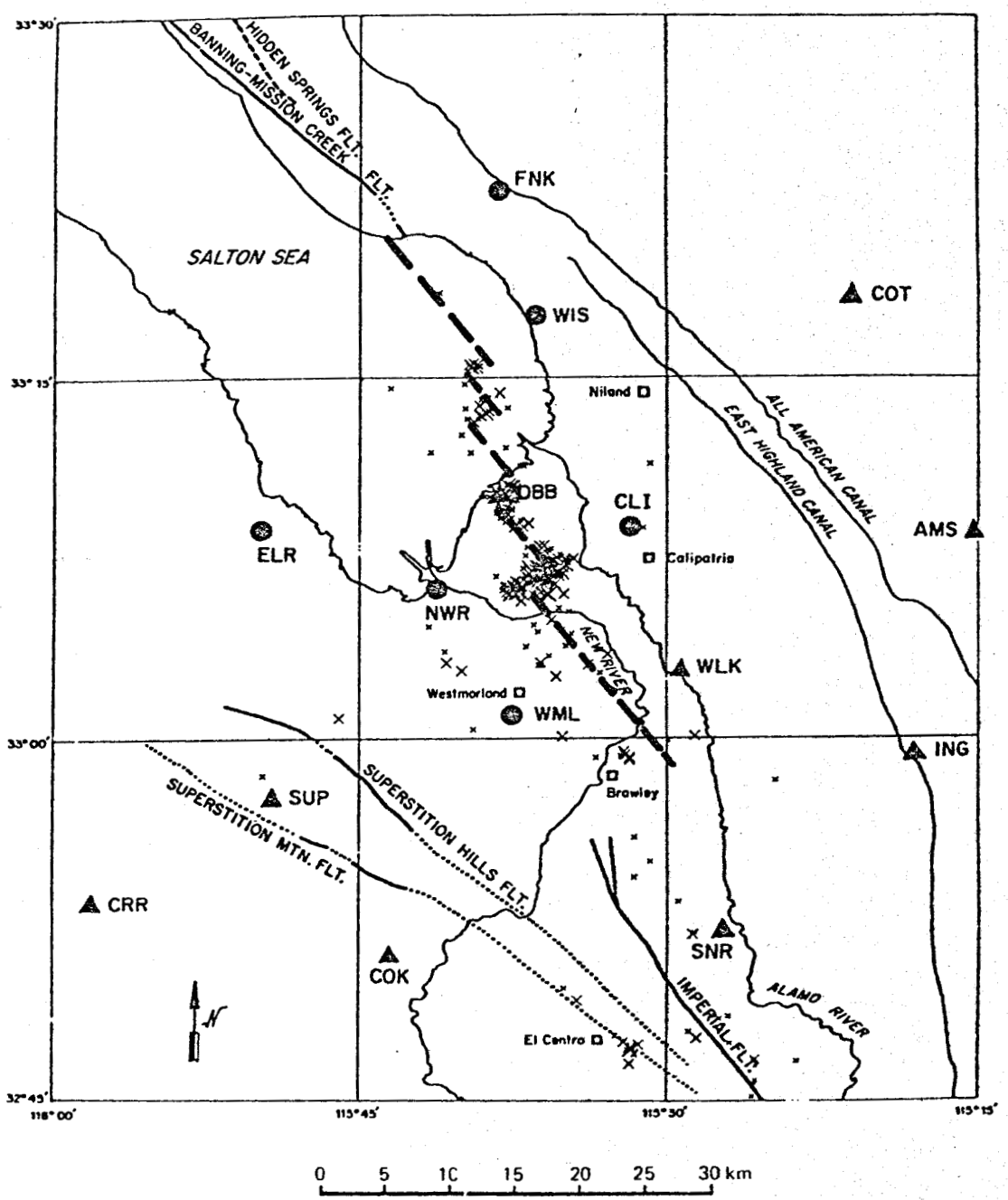

Figure 29

Tentative fault locations based on microearthquake activity occurring near the Salton Sea geothermal area (after Schnapp and Fuis, 1977). Large X denotes epicenter of earthquake with magnitude greater than 3; small x magnitude less than 3. Solid triangles are seismograph stations in the Imperial Valley network installed in 1973. Solid circles are seismograph stations installed in November, 1976.

(3 degrees) and east (7.5 degrees). Extrapolating basement to the west yields a depth of 2 km at Obsidian Butte. Extrapolation of basement to the north (Obsidian Butte) and east (East Highline Canal) yields depths of 5.2 and 5 km, respectively. An extrapolation of basement to the south yields a depth of 6.6 km near Brawley, California, in the center of the Imperial Valley.

A second interpretation of basement is proposed in Model 2 (Figure 28). This interpretation assumes a horizontal basement interface in the E-W direction, and proposes the existence of a seismic velocity gradient in the basement within the geothermal area that increases the apparent velocity from east to west. The amount of increase, based on a calculated linear increase that assumes an initial 6.13 km/sec velocity (consistent with seismic velocity information from Profile 2 (and long-distance shots 1 and 3), is on the order of 15%. The basement depth at Obsidian Butte is 5 km. Extrapolations of basement to the south, north and east were mentioned in the discussion of Model 1.

Extrapolations of basement proposed in Model 1 and Model 2 might be naive, as basement interrogation was limited to areas approximately midway between the forward and reverse shot-points of Profiles 1 and 2 (Figure 3). Arrivals from basement immediately adjacent Obsidian Butte were not observed in the refraction recordings due to the placement of the profile lines. The discrepancy in basement depth at Obsidian Butte (based on extrapolations) in Model 1 (2 km vs. 5.2 km) is a consequence. To obtain such basement arrivals would have required either the extension of the profile lines beyond the present

limits (Figure 3) or moving the shot-point locations. Such changes near Obsidian Butte were all but impossible, due to the limited number of available locations imposed by agricultural activity and accessibility.

To resolve the problem of the basement interpretation in Model 1 and Model 2, additional basement depth determinations are needed near Obsidian Butte. Seismic refraction profiles shot NE-SW along the southern shore of the Salton Sea could provide the necessary basement information needed near Obsidian Butte. Intersections with previous profile lines would provide a check on depth calculations.

DISCUSSION

The seismic interpretations proposed in Model 1 and Model 2 are consistent with results from other geophysical studies that have included the geothermal and adjacent areas. Based on an aeromagnetic study (Griscom and Muffler, 1971), the depth computed to an inferred igneous mass trending NW-SE through the geothermal area (2.1 km near Obsidian Butte) is in agreement with the depth to the basement high proposed in Model 1 (2 km near Obsidian Butte). Inspection of gravity (Figure 30) and aeromagnetic data adjacent Obsidian Butte (Figure 31) shows a similar gradient in the E-W direction, of which the seismic velocity gradient proposed in Model 2 could be an expression. Rough calculations of density contrasts, made assuming the basement interpretations in Model 1 and Model 2 are the cause of the gravity anomaly near Obsidian Butte (Appendix I), yield values of 0.29 gm/cc (Model 1) and 0.11 gm/cc (Model 2). These are consistent with density contrasts proposed by Biehler (1964) based on half-width computations of the gravity anomaly.

The basement depth of 6.6 km near the center of the Imperial Valley proposed in Model 1 and Model 2 is consistent with the depth to basement proposed by Biehler (1964). Biehler obtained a depth of 6 km based upon extrapolation of the Westmoreland profile. Model 1 and Model 2 show a basement depth of approximately 6 km at the point of intersection with the Wesmoreland profile.

In view of the geophysical and geological expressions of the geothermal area (e.g. high heat flow, recent volcanism), it is possible

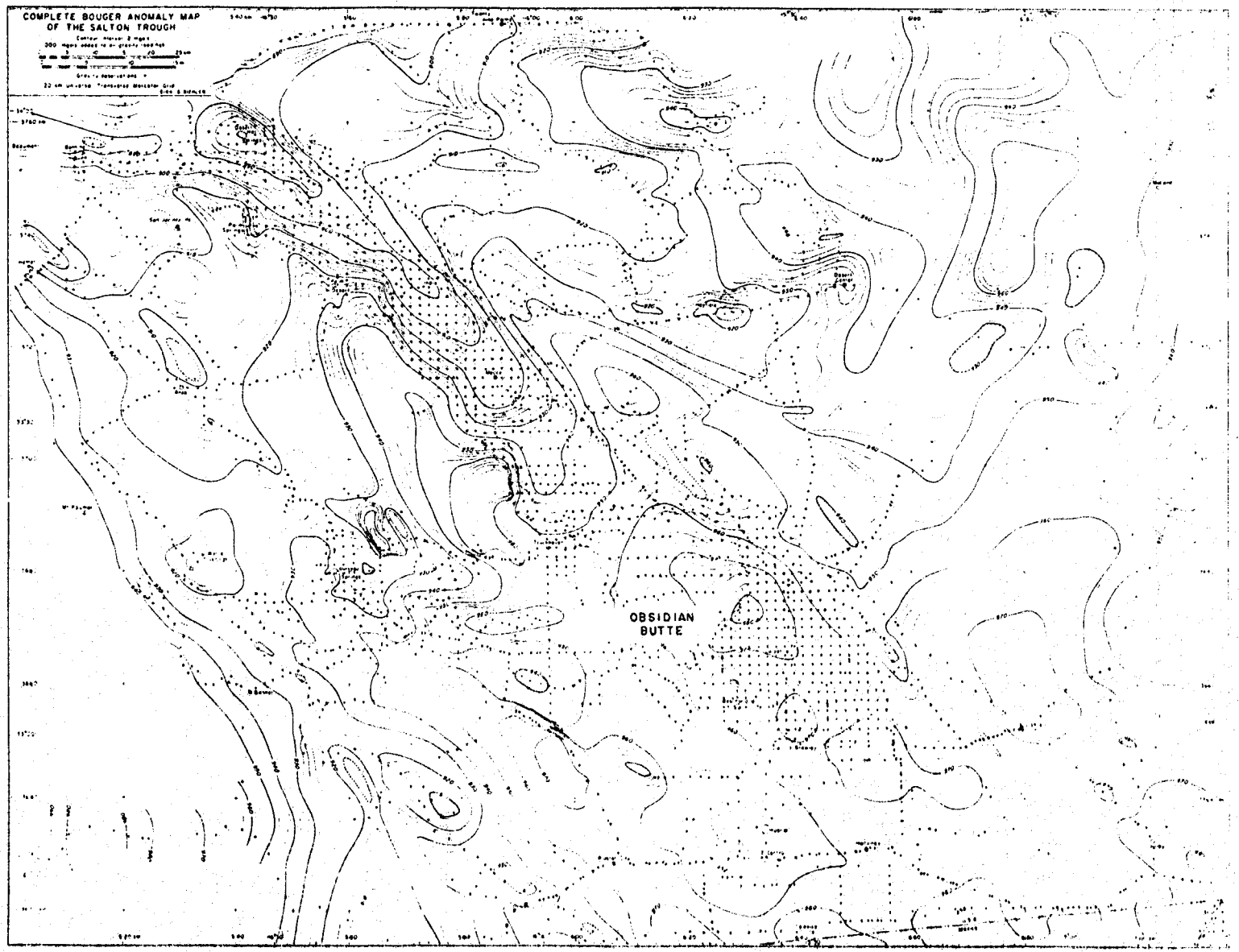

Figure 30

Gravity map of the Salton Trough
(after Biehler, 1964)

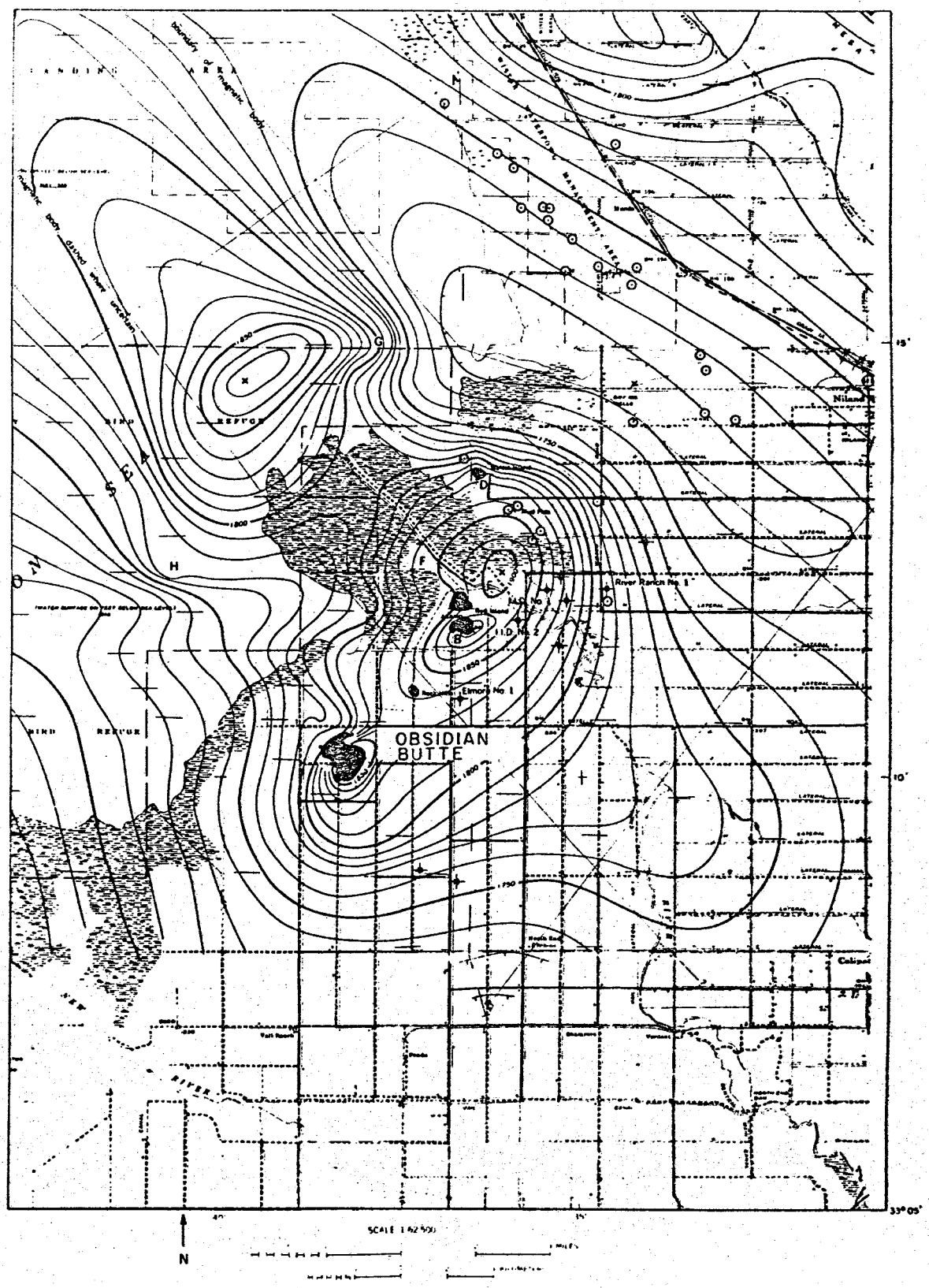

Figure 31

Aeromagnetic map of the Salton Sea geothermal area (after Griscom and Muffler, 1971). Contour interval is 50 gammas.

the interpretations given in Model 1 and Model 2 might be explained by mechanisms involving magmatic activity at depth. The basement high proposed in Model 1 might be the result of uplift caused by the emplacement of magma into the basement beneath the geothermal area. Increasing pressures from expanding gasses and heating could have produced a flexure in basement. An alternative to uplift is that the proposed basement high is part of a large intrusive mass at shallow depth. The seismic velocity gradient proposed in Model 2 might also result from a magmatic process. Ascending magma might produce gradients in parameters that determine seismic velocity (e.g. density, porosity). In a seismic refraction investigation, such gradients could be expressed by a seismic velocity gradient. The creation of an oceanic type crust within the Imperial Valley as a result of ascending basalt magma has been proposed by Elders et al. (1972). This effect might be expressed by a seismic velocity gradient.

SUMMARY OF IMPERIAL VALLEY SEISMIC VELOCITIES

Table 4 presents a summary of seismic velocity models from representative areas of the Imperial Valley (Figure 2 and 3). Sedimentary section seismic velocities reported from areas near the center of the valley (Profiles 1 and 2, Westmoreland and Mexican Border) agree very closely. Agreement of sedimentary section seismic velocities from areas along the eastern margin (East Highline Canal and Frink) and western margin of the valley (Truckhaven and Superstition Hills) is not as pronounced. Basement velocities reported from areas near the center of the valley (Profiles 1 and 2, and Westmoreland, averaging 6.2 km/sec) are higher than those reported from areas along the margins of the valley (East Highline Canal, Frink and Truckhaven, averaging 5.3 km/sec). This suggests that more basic type rocks exist near the center of the valley, as velocities on the order of 6.2 km/sec are consistent with basic rock types (Dobrin, 1960).

TABLE 4

SEISMIC VELOCITIES IN THE IMPERIAL VALLEY

Profile 1	Profile 2	Westmoreland[1]	Mexican Border[2]	E. Highline Canal[3]	Frink[4]	Truckhaven[5]	Superstition Hills[6]
1.70 (.13)	1.70 (.08)	1.70 (.18)	1.85 (.49)	1.75 (.43)	1.85 (.15)	1.67 (.12)	1.72 (0.21)
1.98 (.57)	1.95 (.55)	1.96 (.55)	2.31 (.51)	2.32 (.97)	2.07 (.46)	----	2.13 (0.35)
2.83 (.32)	2.80 (.94)	2.71 (.975)	2.60 (1.19)	2.62 (.26)	3.04 (.43)	2.32 (.26)	2.41 (1.20)
4.05 (2.41)	3.69 (1.15)	3.76 (1.19)	3.63 (1.37)	3.81 (1.42)	4.20 (1.19)	3.69 (.73)	3.26 (1.06)
4.82 (1.4)	5.18 (2.8)	4.70 (2.68)	4.72	----	----	----	4.33
6.13*	6.16*	6.40*		5.5*	5.39*	5.38*	

*Denotes basement velocity

Velocities in km/sec.
(Average Layer Thickness) in km.

1. Biehler (1964)
2. Kovach et al. (1962), profile 5 and 6
3. Kovach et al. (1962), profile 3
4. Biehler (1964)
5. Biehler (1964)
6. Kovach et al. (1962), profiles 4 and 8

SUMMARY AND CONCLUSIONS

This seismic refraction investigation has studied the sedimentary section and basement within the Salton Sea geothermal area. Based on the seismic data, two models of the geothermal and adjacent area are proposed. Model 1 proposes a basement high within the geothermal area that trends parallel to the axis of the Imperial Valley. Model 2 assumes a horizontal basement interface in the E-W direction, and proposes a seismic velocity gradient in the basement within the geothermal area that increased the apparent velocity from east to west on the order of 15%. A mechanism involving magmatic activity at depth might explain the basement high proposed in Model 1 and the seismic velocity gradient proposed in Model 2.

Both seismic models show the sedimentary section of the geothermal and adjacent area is composed of nearly horizontal seismically defined layers. Sedimentary section seismic velocities reported from areas throughout the Imperial Valley are consistent with the sedimentary seismic velocities reported in the geothermal area. In particular, sedimentary seismic velocities reported near the center of the valley agree very closely with the sedimentary seismic velocities of the geothermal area.

Both Model 1 and Model 2 propose a basement dip of 3 degrees to the south, which yields a thickness of sediments of 6.6 km near Brawley, California, in the center of the Imperial Valley.

Basement velocities observed along the center and margins of the Imperial Valley average 6.2 km/sec and 5.3 km/sec, respectively. The occurrence of high basement velocities along the center of the valley

relative to the valley margins is interpreted as the expression of more basic type rocks existing at the valley center.

Based on offsets inferred in the sedimentary seismic layers near Obsidian Butte, two NW-SE trending fault zones are proposed. The respective locations are 3 km east and 2 km south of Obsidian Butte. The discrepancy in the depths of intersecting seismic layers at Obsidian Butte, based on extrapolations, suggests a third fault zone may exist at Obsidian Butte. The two proposed fault zones are consistent with NW-SE trending lineations of epicenters nearby Obsidian Butte, and are in close agreement with two tentative fault locations proposed by Schnapp and Fuis (1977).

Subsequent to the first arrivals in the recording of long-distance refraction shot 3, emergent high amplitude arrivals were observed beginning near 8.2 and 8.6 sec. The arrivals beginning at 8.2 sec are consistent with reflections from basement, and the arrivals beginning at 8.6 sec are consistent with reflections from a horizon at a depth on the order of 21 km. The arrivals beginning at 8.6 sec are interpreted as reflections from the Mohorovicic discontinuity.

REFERENCES

Biehler, S., 1964, A geophysical study of the Salton Trough of southern California, Ph.D. thesis, California Institute of Technology, Pasasena, California 139 pp.

Biehler, S., R. L. Kovach and C. R. Allen, 1964, Geophysical framework of the northern end of the Gulf of California structural province, in T. H. Van Andel and G. G. Shor, Jr., eds., Marine Geology of the Gulf of California--a symposium, Am. Assoc. Petroleum Geologists, Mem. 3, 126-143.

Dibblee, T. W., 1954, Geology of the Imperial Valley region, California, Calif. Div. of Mines Bull. 170, 21-28.

Dobrin, M., 1960, Introduction to Geophysical Prospecting, McGraw Hill, New York, 446 pp.

Dohr, G., 1974, Applied Geophysics, 33-36.

Elders, W. A., R. W. Rex, T. Meidav, P. T. Robinson, and S. Biehler, 1972, Crustal spreading in southern California, Science, 178, 15-24.

Gilpin, B., 1977, A microseismic study of the Salton Sea geothermal area, Imperial Valley, California, M.S. thesis, University of California, Riverside, 83 pp.

Griscom, A., and L. J. P. Muffler, 1971, Aeromagnetic map and interpretation of the Salton Sea geothermal area, California, U.S. Geol. Survey, Map GP-754.

Hadley, D. M., 1978, personal communication and unpublished velocity structure information.

Hill, D., 1975, Earthquakes, active faults, and geothermal areas in Imperial Valley, California, Science, 188, 1306-1308.

Jennings, C. W., 1967, Geologic map of California, 1:250,000 series Salton Sea sheet, Calif. Div. of Mines and Geology.

Jennings, C. W., 1975, Fault map of California, 1:750,000 series, Geologic map no. 1, Calif. Div. of Mines and Geology.

Johnson, C. E., and D. M. Hadley, 1976, Tectonic implications of the Brawley earthquake swarm, Imperial Valley, California, January, 1975, Bull. Seism. Soc. Am., 66, 1133-1143.

Kasameyer, P. A., 1976, Preliminary interpretation of resistivity and seismic refraction data from the Salton Sea geothermal field, Lawrence Livermore Laboratory, UCRL-52115.

Kelley, V. C., and J. L. Soske, Origin of the Salton volcanic domes, Salton Sea, California, Jour. Geol, 44, 496-509.

Kovach, R. L., C. R. Allen and F. Press, 1962, Geophysical investigations in the Colorado delta region, Jour. Geophys. Research, 67, 2845-2871.

Meidav, T., 1969, Application of electrical resistivity and gravimetry in deep geothermal exploration, Institute of Geophysics and Planetary Physics, University of California, Riverside, 19 pp.

Meidav, T., R. West, A. Katzenstein, and Y. Rotstein, 1976, An electrical resistivity survey of the Salton Sea geothermal field, Imperial Valley, California, Lawrence Livermore Laboratory, UCRL-13690, 1 and 2.

Mota, L., 1954, Determination of dips and depths of geologic layers by the seismic refraction method, Geophysics, 19, 242-254.

Muffler, L. J. P., and D. E. White, 1969, Active metamorphism of upper Cenozoic sediments in the Salton Sea geothermal field and the Salton Trough, southeastern California, Geol. Soc. Am. Bull. 80, 157-169.

Phillips, R. P., 1964, Seismic refraction studies in Gulf of California, A.A.P.G., Memoir 3, Marine geology of the Gulf of California, 90-121.

Randall, W., 1974, An analysis of the subsurface structure and stratigraphy of the Salton Sea geothermal anomaly, Imperial Valley, California, Ph.D. thesis, University of California, Riverside, 92 pp.

Robinson, P. T., W. A. Elders, and L. J. P. Muffler, 1976, Quaternary volcanism in the Salton Sea geothermal field, Imperial Valley, California, Geol. Soc. of America Bull., 87, 347-360.

Savage, J. C., D. D. Goodreau, and W. H. Prescott, 1974, Possible fault slip on the Brawley Fault, Imperial Valley, California, Bull. Seim. Soc. Am., 64, 713-716.

Schnapp, M., G. Fuis, 1976, Preliminary catalog of earthquakes in the northern Imperial Valley, October 1, 1976 to December 31, 1976, U.S. Geol. Survey Seismological Laboratory, Pasadena, California, in Lawrence Livermore Laboratory Geothermal Energy Program Status Report, January 1976-January 1977, UCRL-50046-76.

APPENDIX I

CALCULATIONS OF DENSITY CONTRAST

Assuming the proposed basement interpretations of "Model 1" and "Model 2" are responsible for the gravity anomaly near Obsidian Butte, a rough determination of the density contrasts required can be made. Modeling basement as a semi-infinite horizontal slab, $\Delta g = 12.77 \times 10^{-3} \Delta\rho\ Z$, where Δg is in mgal, $\Delta\rho$ in gm/cc, and Z in feet, the density contrast can be determined by solving for $\Delta\rho$. The maximum value of the gravity anomaly is approximately 24 mgal. Given the basement depths near Obsidian Butte shown in "Model 1" and "Model 2" [2 km (6550 ft) and 5 km (16400 ft) respectively], and solving for $\Delta\rho$, yields values of 0.29 gm/cc ("Model 1") and 0.11 gm/cc ("Model 2"). These density contrasts are consistent with values obtained by Biehler (1964) from half-width computations of the gravity anomaly.

APPENDIX II

SUMMARY OF INTERPRETED FIRST ARRIVAL TIMES

Typical precision of first arrival times is ±0.02 sec. Less precise times (±0.05 sec) are indicated by brackets ([ ]).

Distances are accurate to ±0.03 km.

PROFILE 1

FORWARD

Δ(km)	T(sec)	Δ(km)	T(sec)	Δ(km)	T(sec)	Δ(km)	T(sec)
0.21	0.175	2.04	1.165	3.47	1.530	4.82	1.955
0.27	0.205	2.07	1.169	3.51	1.530	4.85	1.968
0.34	0.234	2.10	1.178	3.54	1.542	4.88	1.978
0.40	0.270	2.13	1.184	3.57	1.548		
0.46	0.310			3.60	1.556	4.97	1.994
0.52	0.333	2.13	1.187	3.63	1.564	5.00	2.004
0.58	0.375	2.16	1.196	3.66	1.572	5.03	2.009
0.64	0.385	2.19	1.200	3.69	1.582	5.06	2.016
0.70	0.415	2.22	1.204	3.72	1.591	5.09	2.024
0.76	0.445	2.26	1.210	3.75	1.601	5.12	2.029
0.82	0.460	2.29	1.217			5.15	2.036
0.88	0.480	2.32	1.227	3.75	1.584	5.18	2.048
0.94	0.505	2.35	1.236	3.78	1.588	5.21	2.064
1.01	0.525	2.38	1.246	3.81	1.598	5.24	2.073
1.07	0.560	2.41	1.255	3.84	1.606	5.27	2.084
1.13	0.580	2.44	1.264	3.87	1.616	5.30	2.087
1.19	0.610	2.47	1.276	3.90	1.626		
1.25	0.640			3.93	1.634	6.19	2.300
1.31	0.675	2.50	1.268	3.96	1.640	6.22	2.308
1.37	0.695	2.53	1.277	3.99	1.650	6.25	2.313
1.43	0.730	2.56	1.286	4.02	1.659	6.28	2.321
1.49	0.760	2.59	1.295	4.05	1.666	6.31	2.330
1.55	0.785	2.62	1.305	4.08	1.676	6.34	2.338
1.62	0.800	2.65	1.318			6.37	2.342
		2.68	1.324	4.11	---	6.40	2.350
1.37	0.800	2.71	1.334	4.15	---	6.43	2.358
1.40	0.815	2.74	1.340	4.18	1.729	6.46	2.364
1.43	0.830	2.77	1.345	4.21	1.742	6.49	2.370
1.46	0.845	2.80	1.355	4.24	1.750	6.52	2.379
1.49	0.865	2.83	1.364	4.27	1.761	8.29	---
1.52	0.882			4.30	1.771	8.35	---
1.55	0.899	2.99	1.404	4.33	1.781	8.41	---
0.58	0.916	3.02	1.411	4.36	1.790	8.47	---
1.62	0.935	3.05	1.418	4.39	1.800	8.53	2.885
1.65	0.947	3.08	1.425	4.42	1.812	8.59	2.900
1.68	0.955	3.11	1.431	4.45	1.822	8.66	2.915
1.71	0.965	3.14	1.440			8.72	2.930
		3.17	1.447	4.54	1.863	8.78	2.945
1.80	1.059	3.20	1.452	4.57	1.875	8.84	2.965
1.83	1.079	3.23	1.460	4.60	1.886	8.90	2.970
1.86	1.093	3.26	1.468	4.63	1.902	8.96	2.990
1.89	1.115	3.29	1.473	4.66	1.909	9.02	2.995
1.92	1.133	3.32	1.480	4.69	1.924	9.08	3.910
1.95	1.152			4.72	1.930	9.14	---
1.98	1.159	3.41	1.515	4.75	1.935	9.20	3.030
2.01	1.161	3.44	1.524	4.79	1.946	9.27	3.055

PROFILE 1

FORWARD (cont.)

Δ(km)	T(sec)	Δ(km)	T(sec)	Δ(km)	T(sec)
9.33	3.070	14.57	---	23.74	[6.088]
9.39	3.075	14.63	---	23.80	[6.103]
9.45	3.100	14.69	[4.203]		
9.51	---	14.75	---		
9.57	3.115	14.81	[4.235]		
9.63	3.130	14.87	[4.253]		
9.69	3.140	14.93	[4.263]		
		15.00	[4.268]		
10.09	3.192	15.06	[4.281]		
10.12	---	15.12	---		
10.15	3.212	15.18	[4.313]		
10.18	3.217	15.24	[4.323]		
10.21	3.220	15.30	[4.333]		
10.24	3.222				
10.27	---	18.20	[4.998]		
10.30	3.237	18.26	[5.003]		
10.33	3.242	18.32	[5.008]		
10.36	3.248	18.38	[5.018]		
10.39	---	18.44	[5.023]		
10.42	3.242	18.50	[5.038]		
		18.56	[5.053]		
12.13	[3.690]	18.62	[5.058]		
12.19	---	18.68	[5.073]		
12.25	[3.702]	18.74	[5.078]		
12.31	[3.712]	18.81	[5.093]		
12.37	[3.740]	18.87	[5.103]		
12.44	[3.760]	18.93	[5.113]		
12.50	[3.772]	18.99	[5.118]		
12.56	[3.777]	19.05	[5.153]		
12.62	[3.790]	19.11	[5.158]		
12.68	[3.803]	19.17	[5.178]		
12.74	[3.812]	19.23	[5.183]		
12.80	[3.823]	19.29	[5.193]		
12.86	[3.827]	19.35	[5.198]		
12.92	[3.845]				
12.98	[3.855]	22.95	[5.958]		
		23.01	---		
13.90	[4.073]	23.07	[5.968]		
13.96	[4.085]	23.13	[5.978]		
14.02	[4.093]	23.19	[5.988]		
14.08	[4.098]	23.26	---		
14.14	[4.103]	23.32	---		
14.20	[4.108]	23.38	---		
14.26	[4.143]	23.44	---		
14.32	[4.153]	23.50	[6.043]		
14.39	[4.163]	23.56	---		
14.45	[4.178]	23.62	---		
14.51	[4.188]	23.68	[6.078]		

PROFILE 1

REVERSE

Δ(km)	T(sec)	Δ(km)	T(sec)	Δ(km)	T(sec)	Δ(km)	T(sec)
0.30	0.167	4.11	2.095	7.77	3.160	13.26	[4.134]
0.34	0.188	4.18	---	7.83	3.175	13.32	---
0.37	0.209	4.24	---	7.89	---	13.38	---
0.40	0.228	4.30	---	7.95	3.205	13.44	[4.166]
0.43	0.246	4.36	2.225	8.02	3.230	13.50	[4.169]
0.46	0.266	4.42	2.248	8.08	3.240	13.56	---
0.49	0.288	4.48	2.255	8.14	3.250	13.62	[4.186]
0.52	0.308	4.54	2.270			13.68	---
0.55	0.326	4.60	2.285	10.03	---	13.75	[4.206]
0.58	0.345	4.66	---	10.09	---	13.81	[4.217]
0.61	0.365	4.72	---	10.15	3.645	13.87	[4.226]
0.64	0.385	4.79	2.352	10.21	3.650		
		4.85	2.372	10.27	3.655	14.63	[4.327]
0.85	0.519	4.91	2.390	10.33	3.670	14.69	[4.332]
0.91	0.552	4.97	2.405	10.39	3.680	14.75	[4.347]
0.98	0.590	5.03	---	10.45	3.685	14.81	[4.357]
1.04	0.617			10.52	3.695	14.87	[4.362]
1.10	0.649	5.21	---	10.58	3.705	14.93	[4.367]
1.16	0.687	5.27	---	10.64	3.715	15.00	[4.377]
1.22	0.718	5.33	---	10.70	3.720	15.06	---
1.28	0.749	5.39	---	10.76	3.730	15.12	[4.397]
1.34	0.782	5.46	2.557	10.82	3.740	15.18	[4.407]
1.40	0.812	5.52	2.577	10.88	---	15.24	[4.407]
1.46	0.847	5.58	2.597	10.94	3.765	15.30	[4.412]
1.52	0.879	5.64	2.620	11.00	---	15.36	[4.418]
1.58	0.906	5.70	---	11.06	---	15.42	[4.422]
1.65	0.935	5.76	2.660	11.12	3.805	15.48	---
1.71	0.968	5.82	2.680	11.19	3.815	15.54	[4.447]
1.77	0.996	5.88	---	11.25	---	15.60	[4.452]
1.83	1.029	5.94	---	11.31	3.840	15.67	[4.457]
1.89	1.059	6.00	2.750	11.37	3.855	15.73	[4.470]
1.95	1.092	6.07	---	11.43	3.860		
2.01	1.120	6.13	2.775				
2.07	---	6.19	2.795	12.47	---		
2.13	1.185	6.25	2.820	12.53	---		
2.19	1.213	6.31	---	12.59	---	16.49	[4.608]
2.26	1.253	6.37	2.865	12.65	[4.058]	16.55	[4.613]
		6.43	---	12.71	[4.067]	16.61	[4.618]
3.63	1.925	6.49	---	12.77	[4.072]	16.67	[4.628]
3.69	1.945	6.55	2.920	12.83	---	16.73	[4.633]
3.75	1.973	6.61	2.945	12.83	[4.084]	16.79	[4.638]
3.81	---			12.95	[4.089]	16.85	[4.643]
3.87	2.025	7.53	3.115	13.01	[4.095]	16.92	[4.653]
3.93	2.050	7.59	---	13.08	[4.102]	16.98	---
3.99	2.072	7.65	3.140	13.14	[4.109]	17.04	[4.663]
4.05	---	7.71	3.150	13.20	[4.119]	17.10	[4.668]

PROFILE 1

REVERSE (cont.)

Δ(km)	T(sec)	Δ(km)	T(sec)
17.16	[4.673]	20.09	[5.101]
17.22	[4.678]	20.15	[5.115]
17.28	[4.683]	20.21	[5.133]
17.34	---	20.27	[5.145]
17.40	---	20.33	[5.141]
17.46	[4.713]		
17.53	[4.718]		
17.59	[4.728]		
17.65	[4.738]		
17.71	---		
17.77	[4.758]		
17.83	[4.763]		
17.89	[4.768]		
18.13	---		
18.20	---		
18.26	[4.807]		
18.32	[4.822]		
18.38	[4.827]		
18.44	---		
18.50	[4.847]		
18.56	[4.872]		
18.62	[4.882]		
18.68	[4.902]		
18.74	---		
18.81	---		
18.87	[4.917]		
19.17	[4.956]		
19.23	[4.960]		
19.29	[4.970]		
19.35	[4.982]		
19.41	[4.985]		
19.48	[5.006]		
19.54	[5.009]		
19.60	[5.025]		
19.66	[5.041]		
19.72	[5.052]		
19.78	[5.068]		
19.84	[5.075]		
19.90	[5.078]		
19.96	[5.095]		
20.02	---		

PROFILE 1*

FORWARD		REVERSE			
Δ(km)	T(sec)	Δ(km)	T(sec)	Δ(km)	T(sec)
0.24	0.179	0.40	0.243	3.60	1.714
0.30	0.215	0.43	0.261	3.63	1.725
0.37	0.245	0.46	0.284	3.66	1.733
0.43	0.284	0.49	0.302	3.69	1.740
0.49	0.321	0.52	0.324	3.72	1.749
0.55	0.355	0.55	0.342	3.75	1.753
0.61	0.387	0.58	0.360	3.78	1.758
0.67	0.407	0.61	0.381	3.81	1.769
0.73	0.427	0.64	0.402	3.84	1.775
0.79	0.454	0.67	0.420	3.87	1.781
0.85	0.485	0.70	0.440	3.90	1.790
0.91	0.505	0.73	0.460	3.93	1.795
0.98	---				
1.04	0.569	0.91	0.530	4.15	1.837
1.10	0.586	0.98	0.561	4.21	1.847
1.16	0.607	1.04	0.594	4.27	1.863
1.22	0.632	1.10	0.631	4.33	1.877
1.28	0.666	1.16	0.662	4.39	1.885
1.34	0.687	1.22	0.694	4.45	1.901
1.40	0.720	1.28	0.729	4.51	1.916
1.46	0.750	1.34	0.762	4.57	1.932
1.52	0.774	1.40	---	4.63	1.945
1.58	0.797	1.46	0.830	4.69	1.958
1.65	0.823	1.52	0.862	4.75	1.968
		1.58	0.896	4.82	1.984
2.07	1.033	1.65	0.915	4.88	1.997
2.10	1.054	1.71	0.954	4.94	2.009
2.13	1.071	1.77	0.991	5.00	2.029
2.16	1.091	1.83	1.022	5.06	2.037
2.19	1.109	1.89	1.059	5.12	2.052
2.22	1.119	1.95	1.084	5.18	2.065
2.26	1.124	2.01	1.128	5.24	2.081
2.29	1.138	2.07	1.152	5.30	2.095
2.32	1.148	2.13	1.185	5.36	2.101
2.35	1.156	2.19	1.214	5.43	2.109
2.38	1.171	2.26	1.250	5.49	2.128
2.41	1.178	2.32	1.279	5.55	2.140

PROFILE 2

FORWARD

Δ(km)	T(sec)	Δ(km)	T(sec)	Δ(km)	T(sec)	Δ(km)	T(sec)
0.46	0.300	2.99	---	5.67	2.285	11.46	[3.857]
0.49	0.316	3.05	---	5.70	2.295	11.52	[3.867]
0.52	0.336	3.11	---	5.73	2.301	11.58	[3.882]
0.55	0.351	3.17	1.458	5.76	2.312	11.64	[3.902]
0.58	0.365	3.23	---	5.79	2.325	11.70	[3.912]
0.61	0.383	3.29	---	5.82	2.325	11.76	[3.927]
0.64	0.403	3.35	---	5.85	2.335	11.83	[3.947]
0.67	0.417	3.41	1.568	5.88	2.345	11.89	[3.952]
0.70	0.433	3.47	1.588	5.91	2.355	11.95	[3.967]
0.73	0.441	3.54	1.613			12.01	[3.982]
0.76	0.456	3.60	1.633	6.83	2.607		
0.79	0.468	3.66	1.653	6.86	2.620	15.42	[4.632]
		3.72	1.668	6.89	2.628	15.48	---
0.94	0.560	3.78	1.693	6.92	2.638	15.54	[4.652]
1.01	0.582	3.84	1.713	6.95	2.647	15.60	[4.667]
1.07	---	3.90	1.728	6.98	2.655	15.67	[4.672]
1.13	0.645			7.01	2.660	15.73	[4.687]
1.19	0.670	4.11	1.818	7.04	2.677	15.79	[4.692]
1.25	0.705	4.18	---	7.07	2.690	15.85	[4.712]
1.31	0.735	4.24	1.886	7.10	2.700	15.91	[4.722]
1.37	0.760	4.30	---			15.97	[4.732]
1.43	---	4.36	1.903	9.08	3.286	16.03	[4.747]
1.49	0.825	4.42	1.923	9.11	3.296	16.09	[4.752]
1.55	---	4.48	1.943	9.14	3.306	16.15	---
1.62	0.895	4.54	1.961	9.17	3.316	16.21	[4.782]
1.68	---	4.60	---	9.20	3.321	16.28	[4.787]
1.74	0.955	4.66	---	9.23	3.331	16.34	[4.802]
1.80	1.000	4.72	2.025	9.27	3.341	16.40	[4.812]
1.86	1.020	4.79	2.048	9.30	3.346	16.46	[4.822]
1.92	1.045	4.85	2.068	9.33	3.356	16.52	[4.832]
1.98	1.080	4.91	2.080			16.58	[4.842]
2.04	---	4.97	2.108	10.61	3.687	16.64	[4.847]
2.10	1.112	5.03	2.128	10.67	3.697	16.70	[4.857]
2.16	1.125	5.09	2.141	10.73	3.712	16.76	[4.872]
2.22	1.142	5.15	2.163	10.79	---	16.82	[4.877]
2.29	1.165	5.21	2.183	10.85	3.732		
		5.27	2.200	10.91	3.747	22.92	[6.065]
2.50	1.213	5.33	2.223	10.97	3.762	22.98	[6.090]
2.56	1.233	5.39	2.233	11.03	3.772	23.04	[6.110]
2.62	---	5.46	2.248	11.09	3.792	23.10	[6.120]
2.68	1.278	5.52	2.273	11.16	---	23.16	[6.135]
2.74	1.303			11.22	3.812	23.22	[6.145]
2.80	1.323	5.58	2.255	11.28	---	23.29	[6.155]
2.86	1.338	5.61	2.272	11.34	[3.837]	23.35	[6.165]
2.93	1.368	5.64	2.275	11.40	[3.842]	23.41	[6.175]

PROFILE 2

FORWARD (cont.)

Δ(km)	T(sec)
23.47	[6.185]
23.53	[6.190]
23.59	[6.210]
23.65	[6.220]
23.71	[6.235]
23.77	[6.245]
23.83	[6.260]
23.90	---
23.96	[6.280]
24.02	[6.295]
24.08	[6.305]
24.14	[6.315]
24.20	[6.330]
24.26	[6.340]
26.85	[4.108]
26.91	---
26.97	---
27.03	[4.143]
27.10	[4.158]
27.16	[4.163]
27.22	[4.168]
27.28	[4.198]
27.34	[4.200]
27.40	[4.208]
27.46	[4.228]
27.52	[4.248]
27.58	[4.263]
27.64	[4.283]
27.70	[4.308]
27.77	[4.313]
27.83	[4.328]
27.89	[4.353]

PROFILE 2

REVERSE

Δ(km)	T(sec)	Δ(km)	T(sec)	Δ(km)	T(sec)	Δ(km)	T(sec)
0.58	0.327	3.44	1.799	9.75	3.864	15.12	[5.098]
0.61	0.345	3.47	1.814	9.81	3.874		
0.64	0.355	3.51	1.824	9.88	3.893	17.92	[5.507]
0.67	0.377	3.54	1.834	9.94	3.914	17.98	[5.513]
0.70	---	3.57	1.849	10.00	3.930	18.04	[5.530]
0.73	0.412			10.06	3.933	18.10	[5.548]
0.76	---	3.63	1.847	10.12	3.962	18.17	[5.557]
0.79	0.444	3.66	1.858	10.18	3.987	18.23	[5.562]
0.82	0.459	3.69	1.876	10.24	4.002	18.29	[5.580]
0.85	0.478	3.72	1.893	10.30	4.012	18.35	[5.583]
0.88	0.494	3.75	1.908	10.36	4.025	18.41	[5.600]
0.91	0.510	3.78	1.934	10.42	4.042	18.47	[5.615]
		3.81	1.948	10.48	4.055	18.53	[5.625]
2.16	1.169	3.84	1.962	10.55	4.063	18.59	[5.633]
2.19	1.183	3.87	1.975	10.61	4.076	18.65	---
2.22	1.197	3.90	1.983	10.67	4.094	18.71	[5.648]
2.26	1.208	3.93	1.993	10.73	---	18.77	[5.665]
2.29	1.220	3.96	2.008	10.79	4.137	18.84	[5.682]
2.32	1.238			10.85	---	18.90	[5.693]
2.35	1.250	4.54	2.230	10.91	4.162	18.96	[5.695]
2.38	1.269	3.60	2.255	10.97	4.182	19.02	[5.700]
2.41	1.280	4.66	2.275	11.03	4.192	19.08	[5.715]
2.44	1.295	4.72	2.305	11.09	4.209	19.14	[5.738]
2.47	1.309	4.79	2.326			19.20	[5.757]
2.50	1.325	4.85	2.356	13.90	[4.913]	19.26	[5.752]
		4.91	2.377	13.96	---	19.32	[5.776]
2.56	1.364	4.97	2.403	14.02	---		
2.59	1.369	5.03	2.420	14.08	[4.928]	30.14	[7.476]
2.62	1.388	5.09	2.440	14.14	[4.943]	30.20	[7.484]
2.65	1.403	5.15	2.468	14.20	[4.953]	30.27	---
2.68	1.419	5.21	2.483	14.26	[4.968]	30.33	[7.494]
2.71	1.426	5.27	2.510	14.32	[4.988]	30.39	[7.496]
2.74	1.431	5.33	2.537	14.39	[4.988]	30.45	[7.513]
2.77	1.445	5.99	2.550	14.45	[4.993]	30.51	[7.524]
2.80	1.462	5.46	2.580	14.51	[4.998]	30.57	[7.533]
2.90	1.505	5.52	2.603	14.57	[5.028]	30.63	---
		5.58	2.620	14.63	[5.033]	30.69	---
3.23	1.694	5.64	2.645	14.76	[5.043]	30.75	---
3.26	1.704	5.70	2.665	14.75	[5.048]	30.81	---
3.29	1.724	5.76	2.685	14.81	[5.053]	30.87	---
3.32	1.751	5.82	2.714	14.87	[5.053]	30.94	---
3.35	1.761	5.88	2.728	14.93	[5.068]	31.00	[7.584]
3.38	1.774	5.94	2.750	15.00	[5.088]	31.06	[7.588]
3.41	1.782	9.69	3.849	15.06	---	31.12	[7.588]
						31.18	[7.611]

PROFILE 3

FORWARD

Δ(km)	T(sec)
0.98	0.580
1.04	0.605
1.10	0.625
1.16	0.645
1.22	0.665
1.28	0.690
1.34	---
1.40	0.740
1.46	0.765
1.52	---
1.58	0.815
5.85	2.408
5.91	2.423
5.97	2.468
6.03	2.488
6.10	2.503
6.16	2.528
6.22	2.543
6.28	2.553
6.34	2.573
6.40	2.593
6.52	2.642
6.55	2.662
6.58	2.672
6.61	2.687
6.64	---
6.67	2.707
6.71	2.717
6.74	2.727
6.77	2.737
6.80	2.747
6.83	2.757
6.86	2.767

REVERSE

Δ(km)	T(sec)	Δ(km)	T(sec)
0.64	0.383	3.23	1.746
0.67	0.399	3.29	1.774
0.70	0.418	3.35	1.802
0.73	0.437	3.41	---
0.76	0.453	3.47	1.848
0.79	0.467	3.54	1.863
0.82	0.489	3.60	1.893
0.85	0.517	3.66	1.918
0.88	0.528	3.72	1.944
0.91	0.549	3.78	1.968
0.94	0.568	3.84	1.993
0.98	0.591	3.90	2.011
		3.96	2.048
1.10	0.673	4.02	2.073
1.16	0.708		
1.22	0.741	4.36	2.175
1.28	0.771	4.39	2.190
1.34	0.800	4.42	---
1.40	0.837	4.45	2.220
1.46	0.868	4.48	2.230
1.52	0.903	4.51	2.245
1.58	0.936	4.54	2.257
1.65	0.968	4.57	2.272
1.71	1.002	4.60	2.280
1.77	1.036	4.63	2.295
1.83	---		
1.89	---	4.69	2.310
1.95	---	4.72	2.310
2.01	---	4.75	2.322
2.07	---	4.79	2.330
2.13	---	4.82	2.335
2.19	---	4.85	2.340
2.26	1.299	4.88	2.345
2.32	1.341	4.91	2.350
2.38	1.363	4.94	2.355
2.44	1.378	4.97	---
2.50	1.427	5.00	2.370
		5.03	2.380
2.93	1.603		
2.99	1.648	5.18	2.428
3.05	1.676	5.24	2.443
3.11	1.690	5.30	2.463
3.17	1.720	5.36	2.478

PROFILE 3

REVERSE

Δ(km)	T(sec)
5.43	2.488
5.49	2.503
5.55	2.523
5.61	---
5.67	---
5.73	2.548
5.79	---
5.85	2.563
5.91	2.578
5.97	2.593
6.03	2.603
6.10	---
6.16	2.633
6.22	2.643
6.28	2.653
6.34	---
6.40	---
6.46	---
6.52	2.703

PROFILE 4

FORWARD

Δ(km)	T(sec)	Δ(km)	T(sec)
2.83	1.475	5.88	2.536
2.86	1.492	5.94	2.558
2.90	1.503	6.00	2.582
2.93	1.508	6.07	2.589
2.96	1.528	6.13	2.615
2.99	1.538	6.19	2.632
3.02	1.553	6.25	2.658
3.05	1.565	6.31	2.671
3.08	1.581	6.37	2.689
3.11	1.596		
3.14	1.601	6.55	2.724
3.17	1.608	6.61	2.738
		6.67	2.757
3.35	[1.680]	6.74	---
3.41	[1.706]	6.80	2.785
3.47	[1.716]	6.86	2.802
3.54	---	6.92	2.825
3.60	[1.760]	6.99	2.832
3.66	[1.790]	7.04	2.854
3.72	[1.817]	7.10	2.865
3.78	[1.845]	7.16	2.878
3.84	[1.870]	7.22	2.904
3.90	[1.894]	7.28	2.908
3.96	[1.908]	7.35	2.925
4.02	[1.928]	7.41	2.940
4.08	[1.940]	7.47	2.959
4.15	[1.957]	7.53	2.976
4.21	[1.968]	7.59	2.987
		7.65	3.004
4.97	[2.267]	7.71	3.022
5.03	---	7.77	3.039
5.09	[2.288]	7.83	3.058
5.15	---	7.89	3.071
5.21	[2.327]	7.95	3.090
5.27	[2.339]		
5.33	[2.364]	8.14	3.114
5.39	[2.379]	8.17	3.137
5.46	[2.402]	8.20	3.147
5.52	---	8.23	3.154
5.58	2.437	8.26	3.164
5.64	2.457	8.29	3.179
5.70	2.470	8.32	3.187
5.76	2.490	8.35	3.196
5.82	2.519	8.38	3.208
		8.41	3.217
		8.44	3.227
		8.47	3.237

PROFILE 4

REVERSE

Δ(km)	T(sec)	Δ(km)	T(sec)	Δ(km)	T(sec)
0.06	0.043	2.41	1.344	5.70	2.686
0.09	0.062			5.76	2.719
0.12	0.078	2.86	1.589	5.82	2.727
0.15	0.101	2.93	1.619	5.88	2.742
0.18	0.121	2.99	1.649		
0.21	0.139	3.05	1.674	6.03	2.761
0.24	0.158	3.11	---	6.07	2.766
0.27	0.181	3.17	1.735	6.10	2.776
0.30	0.197	3.23	1.766	6.13	2.781
0.34	0.220	3.29	---	6.16	2.794
0.37	0.246	3.35	1.822	6.19	2.796
0.40	0.266	3.41	1.850	6.22	2.801
		3.47	1.879	6.25	2.806
0.73	0.448	3.54	1.897	6.28	2.813
0.76	0.466	3.60	1.915	6.31	2.818
0.79	0.483	3.66	1.939	6.34	2.826
0.82	0.499	6.72	---	6.37	2.831
0.85	0.521	3.78	2.000		
0.88	0.535	3.84	2.033		
0.91	0.553	3.90	2.063		
0.94	0.572	3.96	2.094		
0.98	0.591	4.02	2.117		
1.01	0.609	4.08	---		
1.04	0.628	4.15	2.172		
1.07	0.642	4.21	2.199		
		4.27	2.223		
1.25	0.744				
1.31	0.772	4.60	2.311		
1.37	0.808	4.66	2.336		
1.43	0.841	4.72	2.361		
1.49	0.874	4.79	---		
1.55	0.905	4.85	---		
1.62	0.926	4.91	2.422		
1.68	0.972	4.97	2.448		
1.74	1.000	5.03	2.473		
1.80	1.030	5.09	2.502		
1.86	1.051	5.15	2.530		
1.92	1.093	5.21	2.552		
1.98	1.125	5.27	2.578		
2.04	1.145	5.33	2.596		
2.16	1.217	5.39	2.609		
2.22	1.251	5.46	2.626		
2.29	1.284	5.52	2.639		
2.35	---	5.58	2.659		
		5.64	2.674		

PROFILE 5

FORWARD

Δ(km)	T(sec)	Δ(km)	T(sec)	Δ(km)	T(sec)
0.55	0.360	3.35	1.753	5.70	2.551
0.61	0.398	3.41	1.776	5.73	2.562
0.67	0.430	3.47	1.793	5.76	2.573
0.73	---	3.54	---	5.79	2.574
0.79	0.499			5.82	2.585
0.85	0.533	3.75	1.894	5.85	2.595
0.91	0.564	3.81	1.915	5.88	2.608
0.98	0.600	3.87	1.937	5.91	2.622
1.04	0.635	3.93	---	5.94	2.634
1.10	0.669	3.99	1.982	5.97	2.648
1.16	0.700	4.05	2.003		
1.22	0.735	4.11	2.027	6.10	2.659
1.28	0.760	4.18	2.051	6.13	2.671
1.34	0.797	4.24	2.076	6.16	2.680
1.40	0.830	4.30	2.102	6.19	2.694
1.46	0.863	4.36	2.122	6.22	2.699
1.52	0.896	4.42	2.165	6.25	2.702
1.58	0.928	4.48	2.179	6.28	2.712
1.65	0.960	4.54	2.201	6.31	2.722
1.71	0.994	4.60	2.220	6.34	2.738
1.77	1.025	4.66	2.240	6.37	2.754
1.83	1.060	4.72	2.257	6.40	2.764
1.89	---	4.79	2.279	6.43	2.771
1.95	---	4.85	2.300		
		4.91	2.320		
2.13	1.248	4.97	2.343		
2.19	1.270	5.03	2.360		
2.26	1.300	5.09	2.376		
2.32	---	5.15	2.394		
2.38	1.357				
2.44	1.387	5.30	2.449		
2.50	1.414	5.33	2.459		
2.56	1.439	5.36	2.467		
2.62	1.465	5.39	2.471		
2.68	1.500	5.43	2.483		
2.74	---	5.46	2.490		
2.80	1.531	5.49	2.503		
2.86	1.559	5.52	2.512		
2.93	1.587	5.55	2.520		
2.99	1.612	5.58	2.530		
3.05	1.634	5.61	2.538		
3.11	1.657	5.64	2.544		
3.17	1.677				
3.23	---	5.64	2.532		
3.29	1.724	5.67	2.538		

PROFILE 6

Δ(km)	T(sec)	Δ(km)	T(sec)
1.92*	1.069	4.54	2.194
1.95*	1.077	4.60	2.219
1.98*	1.096	4.66	2.242
2.01*	1.109	4.72	---
2.04*	1.119		
2.07*	1.139	5.48	2.502
2.10*	1.159	5.54	2.507
2.13*	1.169	5.60	2.517
2.16*	1.189	5.66	2.517
2.19*	1.207	5.72	2.522
2.22*	1.232	5.79	2.532
2.25*	1.241	5.85	2.537
		5.91	2.567
2.40*	1.277	5.97	2.587
2.43*	1.281	6.03	2.607
2.46*	1.298	6.09	2.617
2.49*	1.304	6.15	2.627
2.52*	1.327	6.21	2.642
2.56*	1.344	6.27	2.642
2.59*	1.357	6.33	2.647
2.62*	1.374		
2.65*	1.401		
2.68*	1.406		
2.71*	1.426		
2.74*	1.438		
3.32	1.696		
3.38	1.727		
3.44	1.755		
3.50	---		
3.56	1.804		
3.62	1.833		
3.68	1.867		
3.74	1.896		
3.80	1.923		
3.87	1.946		
3.93	1.968		
3.99	1.993		
4.05	2.014		
4.11	2.039		
4.17	2.059		
4.23	2.086		
4.29	2.107		
4.35	2.124		
4.41	2.149		
4.48	2.167		

*Denotes precision of ±0.10 sec.

PROFILE 5

REVERSE

Δ(km)	T(sec)	Δ(km)	T(sec)	Δ(km)	T(sec)
0.40	0.271	2.07	1.174	5.00	2.440
0.43	0.290	2.13	1.208	5.06	2.458
0.46	0.310	2.19	1.252	5.12	2.476
0.49	0.326	2.26	1.281	5.18	2.495
0.52	0.339	2.32	1.316	5.24	2.512
0.55	0.356	2.38	1.345	5.30	2.532
0.58	0.377	2.44	1.367	5.36	2.551
0.61	0.400	2.50	1.396	5.43	2.570
0.64	0.421	2.56	1.427	5.49	2.589
0.67	0.441	2.62	1.457	5.55	2.610
0.70	0.459	2.68	1.481	5.61	2.627
0.73	0.475	2.74	1.510	5.67	2.649
		2.80	1.540	5.73	2.664
0.85	0.528	2.86	1.575	5.79	2.680
0.88	0.548	2.93	---	5.85	2.694
0.91	0.563	2.99	1.627	5.91	2.703
0.94	0.582	3.05	1.655	5.97	2.714
0.98	0.595	3.11	1.686	6.03	2.730
1.01	0.609			6.10	2.748
1.04	0.627	3.32	1.782	6.16	---
1.07	0.646	3.38	1.804	6.22	2.760
1.10	0.669	3.44	1.836	6.28	2.778
1.13	0.681	3.51	1.861	6.34	---
1.16	0.698	3.57	1.883		
1.19	0.714	3.63	1.910		
		3.69	1.935		
1.22	0.709	3.75	1.968		
1.25	0.730	3.81	1.992		
1.28	0.751	3.87	2.020		
1.31	0.770	3.93	2.046		
1.34	0.790	3.99	2.069		
1.37	0.803	4.05	2.084		
1.40	0.819	4.11	2.121		
1.43	0.834	4.18	2.154		
1.46	0.852	4.24	2.178		
1.49	0.873	4.30	2.203		
1.52	0.892	4.36	2.228		
1.55	0.912	4.42	2.250		
		4.48	2.271		
1.71	---	4.54	---		
1.77	1.021	4.60	2.332		
1.83	1.054	4.66	2.362		
1.89	1.088	4.72	---		
1.95	1.116				
2.01	1.147	4.94	2.421		